2D-REMPI of HBr: Study of singlet & triplet Rydberg states and the ion-pair state

Helgi Rafn Hróðmarsson

Raunvísindadeild
Háskóli Íslands
2011

2D-REMPI of HBr: Study of singlet & triplet Rydberg states and the ion-pair state

Helgi Rafn Hróðmarsson

18 ECTS thesis as a part of
Baccalaureus Scientiarum degree in Chemistry

Supervisors
Prof. Ágúst Kvaran
Gísli Hólmar Jóhannesson, Ph.D.

Faculty of Physical Sciences
School of Engineering and Natural Sciences
University of Iceland
Reykjavík, May 2011

2D-REMPI of HBr
Study of singlet & triplet Rydberg states and the ion-pair state.

18 ECTS thesis as a part of *Baccalaureus Scientiarum* degree in Chemistry

Faculty of Physical Sciences
School of Engineering and Natural Sciences
University of Iceland
VRII, Hjarðarhagi 2-6
107 Reykjavík

Telephone: 525 400

Registration information:
Helgi Rafn Hróðmarsson, 2011, *2D-REMPI of HBr: Study of singlet and triplet Rydberg states and the ion-pair state*, BS thesis, Faculty of Physical Sciences, University of Iceland. 39 pages.

Print: Háskólaprent
Reykjavík, May 2011

Hér með lýsi ég því yfir að ritgerð þessi er samin af mér og að hún hefur hvorki að hluta né í heild verið lögð fram áður til hærri prófgráðu.

I hereby declare that this report is written by me and has not been handed in at part or in whole for a higher education degree.

_____

Helgi Rafn Hróðmarsson

Útdráttur

Fjölljóseindajónun og truflana flugtíma-litrófsgreiningar voru framkvæmdar fyrir tveggja ljóseinda gleypni á HBr á sviðinu 78960 – 79820 cm^{-1} til að mæla litróf $f^3\Delta_1$ (1,0), $F^1\Delta_2$ (1,0), $V^1\Sigma^+$ (m+7) og $H^1\Sigma^+$ (0,0) orkuástandanna. Nýjar gleypnilínur sjást í fyrsta skipti innan $f^3\Delta_1$ (1,0), $F^1\Delta_2$ (1,0) og $V^1\Sigma^+$ (m+7) ástandanna. Truflanaáhrifa á milli $F^1\Delta_2$ (1,0) og $V^1\Sigma^+$ (m+7) eru gerð skil og tilsvarandi truflanareikningar eru framkvæmdir. Sömuleiðis sjást truflanaáhrif á milli $H^1\Sigma^+$ (0,0) ástandsins og $V^1\Sigma^+$ (m+7) og $V^1\Sigma^+$ (m+8) ástandanna, og tilsvarandi truflanareikningar $H^1\Sigma^+$ (0,0) ástandsins framkvæmdir. Línufærslu-greining, jónpara hlutfalls-greining og glæný bandvíddar-greining eru framkvæmdar til staðfestingar á truflanaáhrifum á milli F og V ástandanna annars vegar og H og V ástandanna hins vegar. Staðsetning atómlína er svo loks hagnýtt til útskýringa á frávikum sem eiga sér stað í ákvörðun nýrra gleypnilína og línufærslu-greiningum.

Abstract

Two-photon resonance enhanced multi-photon ionization time-of-flight (REMPI-TOF) analysis was performed for HBr in the region 78960 – 79820 cm^{-1} to obtain 1D REMPI spectra of the $f^3\Delta_1$, $F^1\Delta_2$, $V^1\Sigma^+$ and $H^1\Sigma^+$ states. New line positions are assigned for the $f^3\Delta_1$, $F^1\Delta_2$ and $V^1\Sigma^+$ states for the first time. Near-resonance interaction effects are observed and calculated for interactions between the $F^1\Delta_2$ and $V^1\Sigma^+$ (m+7) states. Perturbation effects are also observed and calculated for interactions between the $H^1\Sigma^+$ state and the V (m+7) and V (m+8) states. Line shift analysis, ion-pair signal intensity ratio analysis (IPSIRA), and last but not least a state-of-the-art bandwidth analysis is successfully performed to confirm near-resonance interaction between the F and V state and perturbation effects between the H and V states. Atomic line positions are finally applied to explain various deviations in assignment and line shift.

Fyrir Ingibjörgu

Index

Index ..... **ix**

Figures ..... **xi**

Tables ..... **xiii**

Acknowledgments ..... **xv**

1 Introduction **1**

2 Experimental **3**
2.1 Uncertainties 3

3 Results and analysis **5**
3.1 Assignment / new peaks 5
3.1.1 The f $^3\Delta_1$ (1,0) Rydberg state 5
3.1.2 The F $^1\Delta_2$ (1,0) Rydberg state 6
3.1.3 The V $^1\Sigma^+$ (m+7) ion-pair state 9
3.1.4 The H $^1\Sigma^+$ (0,0) Rydberg state 10
3.2 Shift analysis 12
3.2.1 The F $^1\Delta_2$ (1,0) Rydberg state 12
3.2.2 The V $^1\Sigma^+$ (m+7) ion-pair state 14
3.3 Ion-pair signal intensity ratio analysis (IPSIRA) 16
3.3.1 The F $^1\Delta_2$ (1,0) Rydberg state 16
3.3.2 The H $^1\Sigma^+$ (0,0) Rydberg state 19
3.4 Bandwidth analysis 23
3.4.1 The F $^1\Delta_2$ (1,0) Rydberg state 23
3.4.2 The V $^1\Sigma^+$ (m+7) ion-pair state 24
3.4.3 The H $^1\Sigma^+$ (0,0) Rydberg state 25
3.5 Atomic lines 27

4 Conclusion **29**

References **31**

5 Appendix **33**

Figures

Figure 3-1 Calculated energy levels for the F and V states. From the calculated energy levels it is clear that some kind of state-state interaction could occur, i.e. the J‘ = 5 peak position of the F state and J‘ = 6 peak position of the V state could be observed at a lower wavenumber and the J‘ = 6 peak position of the F state and the J‘ = 5 peak of the V state could be observed at a higher wavenumber. 13

Figure 3-2 Energy level spacing ($\Delta E_{J',J'-1} = E(J')-E(J'-1)$) as a function of rotational levels, J‘ in the a) 79 isotopomer and the b) 81 isotopomer within the F state. The expected shift of peaks is surprisingly not observed. 14

Figure 3-3 Energy level spacing as a function of rotational levels, J‘ in the a) 79 isotopomer and the b) 81 isotopomer within the V state. The results are not what was to be expected and hint at enormous line shifts within the V state; a trait not shared with the F state. 15

Figure 3-4 Relative ion signal intensities, $I(^{i}Br^{+})/I(H^{i}Br^{+})$ a) i = 79 and b) i = 81 vs. J‘ derived from Q rotational lines of REMPI spectra due to resonance transitions between the F and V states (blue columns) and simulations, assuming J‘ level-to-level interactions between the F state and V state (red columns). 18

Figure 3-5 Calculated energy states for the H and V states. The schematic shows how the calculated energy levels of the H state are „clenched“ between the two V states and how interactions are likely to occur between the energy states. 19

Figure 3-6 Relative ion signal intensities, $I(^{i}Br^{+})/I(H^{i}Br^{+})$ a) i = 79 and b) i = 81 vs. J‘ derived from Q rotational lines of REMPI spectra due to off-resonance transitions between the H state and V states (blue columns) and simulations, assuming J‘ level-to-level interactions between the H state and V states (red column). 22

Figure 3-7 Bandwidth as a function of rotational quantum numbers, J‘ for the $F^{1}\Delta_{2}$ (1,0) state. A significant increase is observed in bandwidth which is indicative of interaction with the $V^{1}\Sigma^{+}$ (m+7) state. 24

Figure 3-8 Bandwidth of H^{+} signals (black), $^{79}Br^{+}$ signals (red) and $^{81}Br^{+}$ signals (blue) as a function of rotational quantum numbers, J‘ for the $V^{1}\Sigma^{+}$ (m+7) state. A clear increase is observed in bandwidth which is indicative of near-resonance interaction with the $F^{1}\Delta_{2}$ (1,0) state 25

Figure 3-9 Bandwidth of the ion signals, $^{i}Br^{+}$ (red) and $H^{i}Br^{+}$ (blue) as a function of the the rotational quantum numbers, J‘. Observed is a slight decrease in the bandwidths of all ion signals from J‘ = 0-4 and a slight increase in bandwidths of all ion signals from J‘ = 4-8. Uncertainty too high for clear evaluation in J‘ = 9. 27

Figure 5-1 Range of the REMPI scan for this particular research and the excited states measured. 33

Figure 5-2 Positions of all rotational quantum states observed in this particular research. 34

Figure 5-3 1D REMPI overview spectrum of the scanned range for this experiment. 35

Figure 5-4 Enlarged view of the HBr REMPI spectrum. Pictured is the $f^3\Delta_1$ (1,0) state. 36

Figure 5-5 Enlarged view of the HBr REMPI spectrum. Pictured are the O, P and Q lines of the $F^1\Delta_2$ (1,0) state and some of the Q lines of the $V^1\Sigma^+$ (m+7) state. 37

Figure 5-6 Enlarged view of the HBr REMPI spectrum. Pictured are the R and S lines of the $F^1\Delta_2$ (1,0) state, the rest of the Q lines of the $V^1\Sigma^+$ (m+7) state, the S lines of the $V^1\Sigma^+$ (m+7) state and some of the O lines of the $H^1\Sigma^+$ (0,0) state. 38

Figure 5-7 Enlarged view of the HBr REMPI spectrum. Pictured are the Q, S and rest of the O lines of the $H^1\Sigma^+$ (0,0) state. 39

Tables

Table 3-1 a) Assignment of peaks within the f $^3\Delta_1$ (1,0) state, b) Calculated energies of assigned rotational quantum states, and c) the mean of the calculated energies of assigned rotational quantum states. The uncertainty is higher for the values J‘ = 1,2 because the standard deviation for the two measurements involved exceeds the uncertainty that was evaluated when the peaks were assigned. Hence, the standard deviation is used for the uncertainty. 6

Table 3-2 Assignment of the O lines within the $F^1\Delta_2$ (1,0) Rydberg state. Peaks at J‘ = 5 are observed for the first time..... 7

Table 3-3 Assignment of the P lines within the $F^1\Delta_2$ (1,0) Rydberg state. Peaks at J‘ = 8-11 are observed for the first time. 7

Table 3-4 Assignment of the Q lines within the $F^1\Delta_2$ (1,0) Rydberg state..... 7

Table 3-5 Assignment of the R lines within the $F^1\Delta_2$ (1,0) Rydberg state. 8

Table 3-6 Assignment of the S lines within the $F^1\Delta_2$ (1,0) Rydberg state. Peaks at J‘ = 7 are observed for the first time..... 8

Table 3-7 Calculated rotational energy levels from values of observed peak positions of the a) 79 isotopomer and b) 81 isotopomer for the F state. The uncertainties of the mean for J‘ = 2-7 are the standard deviations of the measurements since they are greater than the evaluated uncertainty of the peak positions. Other uncertainties are evaluated directly from the uncertainties of the peak positions..... 8

Table 3-8 Assignment of the Q lines within the $V^1\Sigma^+$ (m+7) ion-pair state. Peaks at J‘ = 5- 9 are observed for the first time. 9

Table 3-9 Assignment of the S lines within the $V^1\Sigma^+$ (m+7) ion-pair state. 10

Table 3-10 Calculated rotational energy levels from values of observed peak positions of the a) 79 isotopomer and b) 81 isotopomer for the V state..... 10

Table 3-11 Assignment of the O lines within the $H^1\Sigma^+$ (0,0) Rydberg state. 11

Table 3-12 Assignment of the Q lines within in $H^1\Sigma^+$ (0,0) Rydberg state..... 11

Table 3-13 Assignment of the S lines within the $H^1\Sigma^+$ (0,0) Rydberg state..... 11

Table 3-14 Calculated rotational energy levels from values of observed peak positions of the a) 79 isotopomer and b) 81 isotopomer for the H state..... 12

Table 3-15 Energy difference between the calculated energy levels of the $F^1\Delta_2$ (1,0) state and the $V^1\Sigma^+$ (m+7) state for each rotational quantum number J‘. 16

Table 3-16 Parameter values, relevant to state mixing derived from peak shifts and intensity ratios ($I(^{i}Br^{+})/I(H^{i}Br^{+})$) as a function of J‘. 17

Table 3-17 Energy difference between the calculated energy levels (see expression 3) of the $H^{1}\Sigma^{+}$ (0,0) state and the a) $V^{1}\Sigma^{+}$ (m+7) state for each rotational quantum number J‘ and b) the $V^{1}\Sigma^{+}$ (m+8) state for each rotational quantum number J‘. The values for the V (m+8) state were made available by associate J. Long (work unpublished). 20

Table 3-18 Parameter values, relevant to state mixing of the H state and the V (m+7) and V (m+8) states respectively, derived from peak shifts and intensity ratios ($I(^{i}Br^{+})/I(H^{i}Br^{+})$) as a function of J‘. The interaction strength, W_{12}, is assumed to be approximately half the energy difference between resonance states, $|\Delta E(J'_{res})|$, with a large uncertainty factor. 21

Table 3-19 Bandwidths and corresponding lifetimes of the rotational quantum states, J‘, within the $F^{1}\Delta_{2}$ state. A slight increase in bandwidth is observed around J‘ = 5 as well as a corresponding decrease in lifetime indicative of interaction between the $F^{1}\Delta_{2}$ state and the $V^{1}\Sigma^{+}$ (m+7) state. 23

Table 3-20 Bandwidths and corresponding lifetimes of the rotational quantum states, J‘, within the $V^{1}\Sigma^{+}$ (m+7) state. A gargantuan increase in bandwidth is observed at J‘ = 4-6 and a corresponding decrease in lifetime as well is indicative of interaction between the $F^{1}\Delta_{2}$ state and the $V^{1}\Sigma^{+}$ (m+7) state. 25

Table 3-21 Bandwidths of the $^{i}Br^{+}$ ion signals and corresponding lifetimes of their respective rotational quantum states. An increase in lifetime is observed for J‘ = 4 signifying that perturbation is present from the V states. 26

Table 3-22 Bandwidths of the $H^{i}Br^{+}$ ion signals and corresponding lifetimes of their respective rotational quantum states. An increase in lifetime is observed for J‘ = 4 signifying that perturbation is present from the V states. 26

Table 3-23 Calculated quantum rotational energy levels of the $f\ ^{3}\Delta_{1}$ and $F^{1}\Delta_{2}$ states respectively in the closest vicinity of observed positions of atomic lines. 28

Acknowledgments

This research could not have been done without the invaluable support of Professor Ágúst Kvaran, Victor Huasheng Wang and Yingming Long. I would also like to thank Gísli Hólmar Jóhannesson, Ph.D. for support on reviewing and auditing the thesis.

1 Introduction

Low-resolution vacuum ultraviolet absorption spectra of the hydrogen halides were first reported and studied in 1938 by Price.[1] From that point on, an abundance of spectroscopic data has been derived from high-resolution absorption spectroscopy,[2-12] fluorescent studies,[12,13] as well as from resonance enhanced multiphoton ionization (REMPI) experiments.[14-32] The majority of the work has been on HCl,[4-6,12,14-20,22,23,26-28,30-32] with its hydrogen halide counterparts, HBr,[2,3,9,13,21-23,27-29] and HI,[7,8,11,22-25,27] coming in second and third respectively. The deuteriated halides DCl,[4,5] DBr,[9] and DI[7,8,10] have also been studied to a lesser extent.

One of the reasons why the hydrogen halides are of significant interest is the interaction between Rydberg and valence states (a general characteristic for the hydrogen halides). The strong spin-orbit coupling, arising from the bromine atom, contributes greatly to the spectroscopic interest in the molecule. The molecule has many practical uses, the most substantial of which is usage in organic synthesis as an additive or substitutive element within the pharmaceutical industry. HBr has also been implicated in atmospheric pollution, so data on molecule-photon interaction is of great interest in understanding stratospheric photochemistry as well as being relevant to the photochemistry of planetary atmospheres and the interstellar medium.[12] HBr is also a useful reagent in semiconductor etching.[21]

Resonance enhanced multi-photon ionization (REMPI) is a spectroscopic technique applicable mainly for small molecules and atoms. In practice, a tunable laser is used to access excited intermediate states. In this particular research two-photon resonance excitations are observed, while a third (or in some cases a fourth) photon ionizes the molecule or molecular fragments. A certain nomenclature, *(m+n) REMPI*, is used for the method describing how many photons are absorbed by the chemical of interest, where *m* symbolizes the number of photons needed to access an intermediate state, and *n* symbolizes the number of photons needed to ionize the molecule or molecular fragments.

A Rydberg state of a molecule is a state in which one of the electrons has been excited to a high principal quantum number orbital. Classically, such a state corresponds to putting one electron into an orbit whose dimensions are very large compared to the size of the leftover ion core. Some of the properties of Rydberg states include extreme sensitivity to external influences, extreme reactivity and great probabilities for interactions with microwave radiation.[38] Rydberg state energies follow the Rydberg formula,

$$E_{n,\gamma} = \frac{-Ry}{(n-\mu_\gamma)^2} \quad (1)$$

where n is the pricipal quantum number, Ry is the Rydberg constant for the system, γ represents all of the other quantum numbers, and μ_γ is the quantum defect which describes how much Rydberg states depart from the behaviour of corresponding Rydberg states of the hydrogen atom. Lifetimes of such states are in part a result of the fact that the probability of a spontaneous transition between two states, n_i and n_j ($i < j$), is proportional

to the frequency cubed, ν^3 (a relation derived from the Planck formula by Einstein in 1917).[33]

The ion-pair state $V^1\Sigma^+$ differs from Rydberg states in a very unique way. The potential curve of an ion-pair state exhibits a minimum at a large internuclear distance (~2.5 Å, 2.44 Å for HI and 2.51 Å for HCl, data unavailable for HBr)[34] while internuclear distances of other observed states in this paper ($f^3\Delta_1$, $F^1\Delta_2$, and $H^1\Sigma^+$) do not exceed 1.5 Å[34]. Furthermore, two-photon excitation from $V^1\Sigma^+$ through repulsive states, leads to dissociation of the molecule, forming H^+ and $^iBr^+$ (i = 79, 81) through different pathways while one or two photon excitation from Rydberg states generally leads to a greater formation of H^iBr^+ ions, as discussed in detail elsewhere for HCl.[30,31]

In this particular research both singlet and triplet states are measured. The difference between the two is that singlet states contain a total spin of $\Sigma = 0$. However, for triplet states, the total spin of the molecule is $\Sigma = 1$.

Perturbations due to state-mixing have been reported for HBr previously.[3,13,21,23,27,28] The perturbations appear either as line shifts,[23,27,28] or as intensity and or bandwidth alterations.[23] Comparison has been made for rotational structure in Rydberg and ion-pair states between HCl and HBr[28] and photorupture channels via the F $^1\Delta_2$ Rydberg state have already been proposed for HCl and HBr.[30,31]

By recording ion-mass spectra as a function of laser frequency, 2D REMPI is obtained. With integration of the ion-mass signals (H^+, $^{79}Br^+$, $H^{79}Br^+$, $^{81}Br^+$, and $H^{81}Br^+$) as a function of laser frequency, 1D REMPI spectra are obtained for each respective ion-mass signal. Hence, Rydberg and ion-pair states generally appear in 1D REMPI spectra as sharp peaks in the H^iBr^+ signal and broad peaks in the H^+ and $^iBr^+$ signals respectively (see Figures 5.3-5.7 in Appendix for 1D REMPI spectra).

In this study 2D REMPI spectra were recorded in the region 78960 – 79820 cm^{-1}. Analysis was performed on the $f^3\Delta_1$ (1,0), $F^1\Delta_2$ (1,0), $V^1\Sigma^+$ (m+7), and $H^1\Sigma^+$ (0,0) states. Peaks in the $f^3\Delta_1$ (1,0) state were assigned for the first time. Line shift analysis, ion-signal intensity ratio analysis (IPSIRA) , and bandwidth analysis for state-state interactions between the $F^1\Delta_2$ (1,0) and $V^1\Sigma^+$ (m+7) states were performed and IPSIRA and bandwidth analysis were perfomed on the interaction between the $H^1\Sigma^+$ (0,0) state and the ion-pair states $V^1\Sigma^+$ (m+7) and $V^1\Sigma^+$ (m+8). This is the first time that bandwidth analysis is used quantitatively and qualitatively to determine state interactions so in those respects this is groundbreaking and innovative research. Finally positions of observed atomic lines are used in speculations of various discrepencies primary results convey.

2 Experimental

Two dimensional (2D) REMPI data for jet cooled HBr gas were recorded. Ions were directed into a time-of-flight tube and detected by a micro-channel plate (MCP) detector to record the ion yield as a function of mass and laser radiation wavenumber. The apparatus used is similar to that described elsewhere.[35-37] Tunable excitation radiation in the 224.0 to 225.0 nm wavelength region was generated by Excimer laser-pumped dye laser systems, using a Lambda Physik CoMPex 205 Excimer laser and a Coherent ScanMatePro dye laser. The dye C-503 was used and frequency doubling obtained with a BBO-2 crystal. The repetition rate was typically 10 Hz. The bandwidth of the dye laser beam was about 0.095 cm^{-1}. Typical laser intensity was 0.1-0.3 mJ/pulse. The radiation was focused into an ionization chamber between a repeller and an extractor plate. An undiluted, pure HBr gas sample (Merck-Schuchardt OHG; purity > 99.8%) was used. It was pumped through a 500 μm pulsed nozzle from a typical total backing pressure of about 2.0 – 2.5 bar into the ionization chamber. The pressure in the ionization chamber was lower than 10^{-6} mbar during experiments. The nozzle was kept open for about 200 μs and the laser beam was typically fired 500 μs after opening the nozzle. Ions were extracted into a time-of-flight tube and focused onto an MCP detector, of which the signal was fed into a LeCroy WaveSurfer 44MXs-A, 400 MHz storage oscilloscope as a function of flight time. Average signal levels were evaluated and recorded for a fixed number of laser pulses (typically 100 pulses) to obtain the mass spectra. Mass spectra were primarily recorded in 0.1 cm^{-1} laser wavenumber steps to obtain 2D REMPI spectra. REMPI spectra for certain ions as a function of excitation wavenumber (1D REMPI) were obtained by integrating mass signal intensities for the particular ion. Care was taken to prevent saturation effects as well as power broadening by minimising laser power. Laser calibration was performed by recording an optogalvanic spectrum, obtained from a built-in Neon cell, simultaneously with the recording of the REMPI spectra. Line positions were also compared with the strongest hydrogen bromide rotational lines reported by Callaghan and Gordon.[21] The accuracy of the calibration was found to be about ±4 cm^{-1} on a two-photon wavenumber scale. Intensity drifts during the scan were taken into account, and spectral intensities were corrected for accordingly.

2.1 Uncertainties

Assignment of peak positions was made by taking the mean of 2-4 positions closest to the likeliest position of the peak. The corresponding uncertainty was then evaluated as the standard deviation from the mean.

Uncertainties in all calculations however were calculated with expression 2.

$$\Delta f(x_1, x_2, \dots, x_n) = \sum_{i=1}^{n} \left| \frac{\delta f}{\delta x_i} \right| \Delta x_i \quad (2)$$

3 Results and analysis

3.1 Assignment / new peaks

Heteronuclear diatomic molecules, such as the hydrogen halides, exhibit strong rotation-vibration spectra. The J-selection rule for one photon rotation-vibration transitions in a diatomic molecule is $\Delta J = 0, \pm 1$ (for $J \neq 0$, otherwise $\Delta J = \pm 1$). In this study however, (2+n) REMPI spectra are analysed, which means the considered excited energy states are a result of two-photon excitation. Therefore the spectra exhibit rotation-vibration transitions adhering to $\Delta J = -2, -1, 0, +1, +2$ transitions leaving the spectra henceforth divided into five branches symbolized as O, P, Q, R & S respectively.

The assignment of peaks entailed assigning each peak to a two photon quantum rotational transition from the ground state ($X^1\Sigma^+$) to an excited state ($f^3\Delta_1$ (1,0), $F^1\Delta_2$ (1,0), $V^1\Sigma^+$ (m+7), or the $H^1\Sigma^+$ (0,0) state). By calculating the energy levels of the excited states from observed peak positions in the 1D REMPI spectrum, assignments were made by using least squares analysis for the best fit for each individual peak to a certain quantum rotational transition.

3.1.1 The f $^3\Delta_1$ (1,0) Rydberg state

The $f^3\Delta_1$ (1,0) state has previously been reported[21], but its rotational quantum states have never been assigned. This is due to the fact the all of the lines are very weak and barely stand out of the background (see Figures 5.3 and 5.4 in Appendix for spectra). Because these lines are very weak, no O or S lines are visible and no detailed analysis could be performed except for the assignment.

Energy levels of the $f^3\Delta_1$ (1,0) state were calculated from the 1D REMPI spectrum with the expression

$$E(J') = \bar{\nu} + E(J'') \quad (3)$$

where E(J‘) is the energy level of the excited state, $\bar{\nu}$ is the observed line position and E(J‘‘) is the corresponding energy level of the ground state from which the molecule was excited and is calculated with the expression

$$E(J'') = B_e * J''(J''+1) - D_e * J''^2(J''+1)^2 \quad (4)$$

where B_e is the rotational constant, D_e is the centrifugal distortion constant (a correctional factor for the rigid rotor model), and J‘‘ is the rotational quantum number of the ground state from which the molecule is excited. For HBr the values of B_e and D_e are 8.348244 cm^{-1} and 3.316573864 * 10^{-4} respectively.[39]

Example of energy level calculation for the observed Q line for the transition $f^3\Delta_1 \leftarrow X^1\Sigma^+$ (v‘ = 1, v‘‘ = 0), (J‘ = 1, J‘‘ = 1) for the 79 isotopomer:

$$E(J'') = 8.348244\,cm^{-1} * 1 * (1+1) - 3.316573864 * 10^{-4} cm^{-1} * 1^2(1+1)^2$$

$$\approx 16.7\ cm^{-1}$$

$$E(J') = 78990.2\,cm^{-1} + 16.7\ cm^{-1} = 79007.2\ cm^{-1}$$

Table 3-1 a) Assignment of peaks within the f $^3\Delta_1$ (1,0) state, b) Calculated energies of assigned rotational quantum states, and c) the mean of the calculated energies of assigned rotational quantum states. The uncertainty is higher for the values J‘ = 1,2 because the standard deviation for the two measurements involved exceeds the uncertainty that was evaluated when the peaks were assigned. Hence, the standard deviation is used for the uncertainty.

a)

J‘	*79 isotopomer [cm^{-1}]*			*81 isotopomer [cm^{-1}]*		
	P line	*Q lines*	*R lines*	*P lins*	*Q lines*	*R lines*
0	78977.7 ± 0.3			78977.3 ± 0.3		
1		78990.2 ± 0.5	79011.6 ± 0.5		78990.5 ± 0.5	79011.8 ± 0.5
2		78994.6 ± 0.5	79024.2 ± 0.3		78994.9 ± 0.5	79023.8 ± 0.3
3		79001.7 ± 0.3			79002.1 ± 0.3	
4		79020.2 ± 0.3			79020.4 ± 0.5	

b)

J‘	*79 isotopomer [cm^{-1}]*			*81 isotopomer [cm^{-1}]*		
	P line	*Q lines*	*R lines*	*P line*	*Q lines*	*R lines*
0	78994.4 ± 0.3			78994.0 ± 0.3		
1		79007.2 ± 0.5	79011.6 ± 0.5		79007.5 ± 0.5	79011.8 ± 0.5
2		79045.0 ± 0.5	79040.9 ± 0.3		79045.3 ± 0.5	79040.5 ± 0.3
3		79102.3 ± 0.3			79102.7 ± 0.3	
4		79187.0 ± 0.3			79187.2 ± 0.5	

c)

J‘	*Mean - 79 isotopomer [cm^{-1}]*	*Mean - 81 isotopomer [cm^{-1}]*
0	78994.4 ± 0.3	78994.0 ± 0.3
1	79009 ± 2	79010 ± 2
2	79043 ± 2	79043 ± 2
3	79102.3 ± 0.3	79102.7 ± 0.3
4	79187.0 ± 0.3	79187.2 ± 0.5

3.1.2 The F $^1\Delta_2$ (1,0) Rydberg state

The spectrum of the F state in HBr does resemble its counterpart within the HCl molecule[30] so further analysis for HBr should therefore make for an interesting comparison with results from HCl analysis (not applied in this thesis however).

Assignment of the F state was simpler than for the triplet state because most of the peaks have been previously reported so it was mearly a question of comparison with the original data reported by Callaghan and Gordon.[21] New peaks were confirmed by calculating the corresponding energy levels in the same way as for the triplet state.

Table 3-2 Assignment of the O lines within the $F^1\Delta_2$ (1,0) Rydberg state. Peaks at J‘ = 5 are observed for the first time.

J‘	*79 isotopomer [cm^{-1}]*	*81 isotopomer [cm^{-1}]*	*Others[21] [cm^{-1}]*
2	79190.1 ± 0.6	79189.9 ± 0.9	79186.7
3	79154.7 ± 1.0	79154.3 ± 1.0	79151.6
4	79120.9 ± 0.4	79121.4 ± 0.9	79115.2
5	79086.2 ± 0.7	79084.8 ± 0.8	
6	79048.6 ± 0.9	79048.6 ± 0.5	79042.1

Table 3-3 Assignment of the P lines within the $F^1\Delta_2$ (1,0) Rydberg state. Peaks at J‘ = 8-11 are observed for the first time.

J‘	*79 isotopomer [cm^{-1}]*	*81 isotopomer [cm^{-1}]*	*Others[21] [cm^{-1}]*
2	79259.4 ± 0.5	79259.0 ± 0.5	79254.5
3	79237.8 ± 0.4	79237.5 ± 0.5	79235.6
4	79218.0 ± 0.4	79217.8 ± 0.4	79215.8
5	79197.8 ± 0.9	79197.4 ± 0.7	79193.5
6	79176.4 ± 1.0	79176.2 ± 0.9	79173.6
7	79155.1 ± 0.5	79154.9 ± 0.8	79151.6
8	79134.4 ± 0.7	79134.2 ± 0.8	
9	79112.2 ± 0.6	79111.5 ± 0.5	
10	79087.4 ± 0.8	79086.9 ± 0.4	
11	79060.1 ± 0.5	79059.7 ± 0.5	

Table 3-4 Assignment of the Q lines within the $F^1\Delta_2$ (1,0) Rydberg state.

J‘	*79 isotopomer [cm^{-1}]*	*81 isotopomer [cm^{-1}]*	*Others[21] [cm^{-1}]*
2	79310.8 ± 0.4	79310.4 ± 0.4	79304.4
3	79308.5 ± 0.3	79308.2 ± 0.4	79302.2
4	79305.2 ± 0.5	79304.8 ± 0.5	79299.4
5	79301.4 ± 0.5	79300.8 ± 0.5	79295.4
6	79298.3 ± 0.6	79298.0 ± 0.6	79292.1
7	79291.8 ± 0.6	79291.5 ± 0.5	79285.7
8	79285.3 ± 0.9	79284.9 ± 0.6	79279.2
9	79277.9 ± 1.0	79277.4 ± 1.0	79271.5
10	79268.8 ± 0.5	79271.4 ± 1.0	79263.1

Table 3-5 Assignment of the R lines within the $F^1\Delta_2$ (1,0) Rydberg state.

J'	*79 isotopomer [cm^{-1}]*	*81 isotopomer [cm^{-1}]*	*Others[21] [cm^{-1}]*
2	79344.0 ± 0.4	79343.7 ± 0.5	79337.8
3	79357.7 ± 0.4	79357.4 ± 0.5	79352.2
4	79369.7 ± 0.4	79369.4 ± 0.5	79365.4
5	79380.8 ± 0.5	79380.5 ± 0.4	79378.2
6	79392.9 ± 0.5	79392.1 ± 0.5	79389.8
7	79404.1 ± 1.0	79403.8 ± 0.8	79400.8

Table 3-6 Assignment of the S lines within the $F^1\Delta_2$ (1,0) Rydberg state. Peaks at J' = 7 are observed for the first time.

J'	*79 isotopomer [cm^{-1}]*	*81 isotopomer [cm^{-1}]*	*Others[21] [cm^{-1}]*
2	79359.7 ± 0.4	79359.4 ± 0.5	79354.4
3	79387.6 ± 0.4	79387.3 ± 0.4	79384.9
4	79418.1 ± 0.6	79417.8 ± 0.5	79415.2
5	79446.9 ± 0.7	79446.6 ± 0.9	79444.6
6	79477.4 ± 1.1	79477.6 ± 1.0	79471.8
7	79506.8 ± 0.7	79506.4 ± 0.7	

Table 3-7 Calculated rotational energy levels from values of observed peak positions of the a) 79 isotopomer and b) 81 isotopomer for the F state. The uncertainties of the mean for J' = 2-7 are the standard deviations of the measurements since they are greater than the evaluated uncertainty of the peak positions. Other uncertainties are evaluated directly from the uncertainties of the peak positions.

a)

J'	*O lines [cm^{-1}]*	*P lines [cm^{-1}]*	*Q lines [cm^{-1}]*	*R lines [cm^{-1}]*	*S lines [cm^{-1}]*	*Mean [cm^{-1}]*
2	79356.9 ± 0.6	79359.6 ± 0.5	79360.8 ± 0.4	79360.7 ± 0.4	79359.7 ± 0.4	79359.5 ± 1.4
3	79404.8 ± 1.0	79404.6 ± 0.4	79408.6 ± 0.3	79407.7 ± 0.4	79404.4 ± 0.4	79406 ± 2
4	79471.0 ± 0.4	79468.1 ± 0.4	79472.1 ± 0.5	79469.8 ± 0.4	79468.1 ± 0.6	79470 ± 2
5	79552.6 ± 0.7	79547.9 ± 0.9	79551.6 ± 0.5	79547.7 ± 0.5	79547.0 ± 0.7	79549 ± 2
6	79648.0 ± 0.9	79642.9 ± 1.0	79648.4 ± 0.6	79643.0 ± 0.5	79644.2 ± 1.1	79645 ± 2
7		79754.4 ± 0.5	79758.3 ± 0.6	79754.2 ± 1.0	79757.0 ± 0.7	79756 ± 2
8		79883.0 ± 0.7	79884.7 ± 0.9			79883.8 ± 1.1
9		80026.4 ± 0.6	80026.6 ± 1.1			80026.5 ± 1.3
10		80183.6 ± 0.8	80183.1 ± 0.9			80183.3 ± 1.0
11		80354.4 ± 0.5				80354.4 ± 0.5

b)

J'	*O lines [cm^{-1}]*	*P lines [cm^{-1}]*	*Q lines [cm^{-1}]*	*R lines [cm^{-1}]*	*S lines [cm^{-1}]*	*Mean [cm^{-1}]*
2	79356.7 ± 0.9	79359.2 ± 0.5	79360.5 ± 0.4	79360.4 ± 0.5	79359.4 ± 0.5	79359.2 ± 1.4
3	79404.4 ± 1.0	79404.3 ± 0.5	79408.3 ± 0.4	79407.4 ± 0.5	79404.0 ± 0.4	79406 ± 2
4	79471.5 ± 0.9	79467.9 ± 0.4	79471.7 ± 0.5	79469.5 ± 0.5	79467.9 ± 0.5	79470 ± 2
5	79551.3 ± 0.8	79547.5 ± 0.7	79551.0 ± 0.5	79547.4 ± 0.4	79546.7 ± 0.9	79549 ± 2
6	79648.0 ± 0.5	79642.7 ± 0.9	79648.1 ± 0.6	79642.2 ± 0.5	79644.5 ± 1.0	79645 ± 3
7		79754.2 ± 0.8	79757.9 ± 0.5	79753.9 ± 0.8	79756.6 ± 0.7	79756 ± 2
8		79882.8 ± 0.8	79884.3 ± 0.6			79883.5 ± 1.0
9		80025.7 ± 0.5	80026.1 ± 1.0			80025.9 ± 1.1
10		80183.1 ± 0.4	80185.7 ± 1.0			80184.4 ± 1.0
11		80354.0 ± 0.5				80354.0 ± 0.5

3.1.3 The V $^1\Sigma^+$ (m+7) ion-pair state

The $V^1\Sigma^+$ (m+7) ion-pair state is quite elusive. Five new peaks have been assigned to the V state but the peaks for J' = 5,6 respectively almost seem to disappear which indicates a close interaction with the nearby F state. Because of the low and almost non-existent intensity of these two peaks, the uncertainty factor increases both in terms of assignment and further analysis. On top of that, the difference between peak positions for the two isotopomers dissipates, i.e. no distinguishable difference is detected between positions of the 79 and 81 isotopomer peak positions.

By assuming preproposed ionization channels for HBr to be (nearly) equivalent with HCl,[30,31] then assignment of the V state is quite obvious since a major characteristic in the V state is its ionization channel in which interaction with repulsive states generates dissociation of the molecule so intensity in the H^+ and $^iBr^+$ signals are far greater than those of H^iBr^+.

Table 3-8 Assignment of the Q lines within the $V^1\Sigma^+$ (m+7) ion-pair state. Peaks at J' = 5- 9 are observed for the first time.

J'	*79 isotopomer [cm^{-1}]*	*81 isotopomer [cm^{-1}]*	*Others[21] [cm^{-1}]*
0	79483.1 ± 0.6	79482.5 ± 0.7	79480.3
1	79474.2 ± 0.6	79473.5 ± 0.6	79471.8
2	79457.0 ± 0.7	79456.2 ± 0.8	79455.6
3	79433.0 ± 1.4	79432.4 ± 1.0	79429.6
4	79399 ± 3	79399 ± 3	79392.3
5	79345 ± 5	79345 ± 5	
6	79284 ± 4	79284 ± 4	
7	79218 ± 2	79218 ± 2	
8	79146.4 ± 1.3	79146.4 ± 1.3	
9	79067.7 ± 1.5	79067.7 ± 1.5	

Table 3-9 Assignment of the S lines within the $V^1\Sigma^+$ (m+7) ion-pair state.

J'	*79 isotopomer [cm^{-1}]*	*81 isotopomer [cm^{-1}]*	*Others[21] [cm^{-1}]*
2	79510.0 ± 1.0	79510.0 ± 1.0	79505.4
3	79520 ± 2	79520 ± 2	79514.9

Table 3-10 Calculated rotational energy levels from values of observed peak positions of the a) 79 isotopomer and b) 81 isotopomer for the V state.

a)

J'	*Q lines [cm^{-1}]*	*S lines [cm^{-1}]*	*Mean [cm^{-1}]*
0	79483.1 ± 0.6		79483.1 ± 0.6
1	79490.9 ± 0.6		79490.9 ± 0.6
2	79507.0 ± 0.7	79510.0 ± 1.0	79508.5 ± 1.5
3	79533.2 ± 1.0	79537 ± 2	79535± 2
4	79566 ± 3		79566 ± 3
5	79595 ± 5		79595 ± 5
6	79634 ± 4		79634 ± 4
7	79685 ± 2		79685 ± 2
8	79745.8 ± 1.3		79745.8 ± 1.3
9	79816.3 ± 1.5		79816.3 ± 1.5

b)

J'	*Q lines [cm^{-1}]*	*S lines [cm^{-1}]*	*Mean [cm^{-1}]*
0	79482.5 ± 0.7		79482.5 ± 0.7
1	79490.2 ± 0.6		79490.2 ± 0.6
2	79506.3 ± 0.8	79510.0 ± 1.0	79508 ± 2
3	79532.6 ± 1.0	79537 ± 2	79535 ± 2
4	79566 ± 3		79566 ± 3
5	79595 ± 5		79595 ± 5
6	79634 ± 4		79634 ± 4
7	79685 ± 2		79685 ± 2
8	79745.8 ± 1.3		79745.8 ± 1.3
9	79816.3 ± 1.5		79816.3 ± 1.5

3.1.4 The H $^1\Sigma^+$ (0,0) Rydberg state

The $H^1\Sigma^+$ Rydberg state is a bit different from its F state counterpart in the sense that only O, Q and S lines are observed. This is due to the fact that the H state is an $\Omega = 0$ state and therefore complies only to $\Delta J = 0, \pm 2$ selection rules. This is due to the fact that subsequently after one photon excitation the molecule enters „a virtual state“, in which normal selection rules apply. Sequentially after the absorbtion of the second photon however, the molecule is further excited from this virtual state to the H state. Therefore lines applicable for $\Delta J = \pm 1$ are eliminated by the crossing of this virtual state.

Assignment of the $H^1\Sigma^+$ state was fairly easy since all observed peaks have been reported previously[21].

Table 3-11 Assignment of the O lines within the $H^1\Sigma^+$ (0,0) Rydberg state.

J'	*79 isotopomer [cm^{-1}]*	*81 isotopomer [cm^{-1}]*	*Others[21] [cm^{-1}]*
0	79597.0 ± 1.0	79596.6 ± 0.7	79595.3
1	79563.2 ± 0.5	79563.2 ± 0.5	79559.3
2	79526.9 ± 0.7	79526.8 ± 0.6	79520.8
3	79483.1 ± 0.6	79483.1 ± 0.6	79480.3
4	79439.7 ± 0.5	79439.6 ± 0.4	79437.1
5	79395.7 ± 0.5	79395.6 ± 0.6	79392.3
6	79352.7 ± 0.5	79352.8 ± 0.6	79346.4

Table 3-12 Assignment of the Q lines within in $H^1\Sigma^+$ (0,0) Rydberg state.

J'	*79 isotopomer [cm^{-1}]*	*81 isotopomer [cm^{-1}]*	*Others[21] [cm^{-1}]*
0	79646.8 ± 0.7	79646.4 ± 0.7	79645.5
1	79644.1 ± 0.6	79644.0 ± 0.5	79643.0
2	79638.8 ± 0.5	79638.8 ± 0.5	79637.6
3	79631.2 ± 0.5	79631.2 ± 0.5	79630.0
4	79623.0 ± 0.2	79622.9 ± 0.4	79620.4
5	79612.7 ± 0.5	79612.5 ± 0.5	79608.6
6	79600.6 ± 0.7	79600.4 ± 0.6	79595.3
7	79584.8 ± 0.5	79584.8 ± 0.5	79579.6
8	79566.5 ± 0.6	79566.3 ± 0.7	79561.3
9	79541.2 ± 1.2	79541.0 ± 1.2	79536.4

Table 3-13 Assignment of the S lines within the $H^1\Sigma^+$ (0,0) Rydberg state.

J'	*79 isotopomer [cm^{-1}]*	*81 isotopomer [cm^{-1}]*	*Others[21] [cm^{-1}]*
2	79687.9 ± 1.1	79687.7 ± 0.9	79688.0
3	79713.9 ± 0.5	79713.9 ± 0.5	79713.9
4	79739.2 ± 0.6	79739.0 ± 0.9	79737.3
5	79764.0 ± 0.5	79764.0 ± 0.5	79759.3
6	79784.3 ± 0.4	79784.2 ± 0.2	79778.8
7	79801.9 ± 0.5	79801.8 ± 0.6	79796.3
8	79816.4 ± 0.4	79816.2 ± 0.4	79810.3

Table 3-14 Calculated rotational energy levels from values of observed peak positions of the a) 79 isotopomer and b) 81 isotopomer for the H state.

a)

J'	*O lines [cm^{-1}]*	*Q lines [cm^{-1}]*	*S lines [cm^{-1}]*	*Mean [cm^{-1}]*
0	79647.1 ± 1.0	79646.8 ± 0.7		79647.0 ± 1.4
1	79663.4 ± 0.5	79660.8 ± 0.6		79662.1 ± 0.6
2	79693.7 ± 0.7	79688.9 ± 0.5	79687.9 ± 1.1	79690 ± 3
3	79733.2 ± 0.6	79731.4 ± 0.5	79730.6 ± 0.5	79731.7 ± 1.1
4	79789.7 ± 0.5	79789.8 ± 0.2	79789.3 ± 0.6	79789.6 ± 0.7
5	79862.1 ± 0.5	79862.9 ± 0.5	79864.1 ± 0.5	79863.0 ± 0.8
6	79952.1 ± 0.5	79950.6 ± 0.7	79951.2 ± 0.4	79951.3 ± 0.9
7		80051.3 ± 0.5	80052.0 ± 0.5	80051.6 ± 0.5
8		80165.9 ± 0.6	80166.4 ± 0.4	80166.2 ± 0.5
9		80289.8 ± 1.2		60289.8 ± 1.2

b)

J'	*O lines [cm^{-1}]*	*Q lines [cm^{-1}]*	*S lines [cm^{-1}]*	*Mean [cm^{-1}]*
0	79646.7 ± 0.7	79646.4 ± 0.7		79646.6± 1.0
1	79663.4 ± 0.5	79660.7 ± 0.5		79662.1 ± 0.4
2	79693.6 ± 0.6	79688.9 ± 0.5	79687.7 ± 0.9	79690 ± 3
3	79733.2 ± 0.6	79731.3 ± 0.5	79730.6 ± 0.5	79731.7 ± 1.1
4	79789.6 ± 0.4	79789.7 ± 0.4	79789.1 ± 0.9	79789.5 ± 1.2
5	79862.0 ± 0.6	79862.7 ± 0.5	79864.1 ± 0.5	79862.9 ± 0.9
6	79952.2 ± 0.6	79950.4 ± 0.6	79951.1 ± 0.2	79951.2 ± 0.9
7		80051.3 ± 0.5	80051.9 ± 0.6	80051.6 ± 0.6
8		80165.7 ± 0.7	80166.2 ± 0.4	80166.0 ± 0.6
9		80289.6 ± 1.2		60289.6 ± 1.2

3.2 Shift analysis

3.2.1 The F $^1\Delta_2$ (1,0) Rydberg state

Shift analysis refers to shifts in peak positions from expected values (abberations from linearity). According to calculated energy levels derived from the Q lines of the F state and Q lines of the V state it is apparent that near resonance interaction is likely to occur (Figure 3.1). Positions of the J' = 5,6 rotational lines in the V state are between the J' = 5,6 rotational lines in the F state so a deviation in the energy level spacing for the two states can be expected.

To a first approximation, energy difference between adjacent unperturbed energy levels increases linearly with J'. To quantitatively determine this line shift, a linear plot of the unperturbed energy levels is acquired. This is done by finding the best linear fit through the least perturbed energy levels (J' = 3, 4, 9, 10) and comparing with the observed values. Abberations from linearity for the observed values should then confirm the perturbation.

However, what is surprisingly observed is what appears to be no clear line shift in the F state for either isotopomer (Figure 3.2).

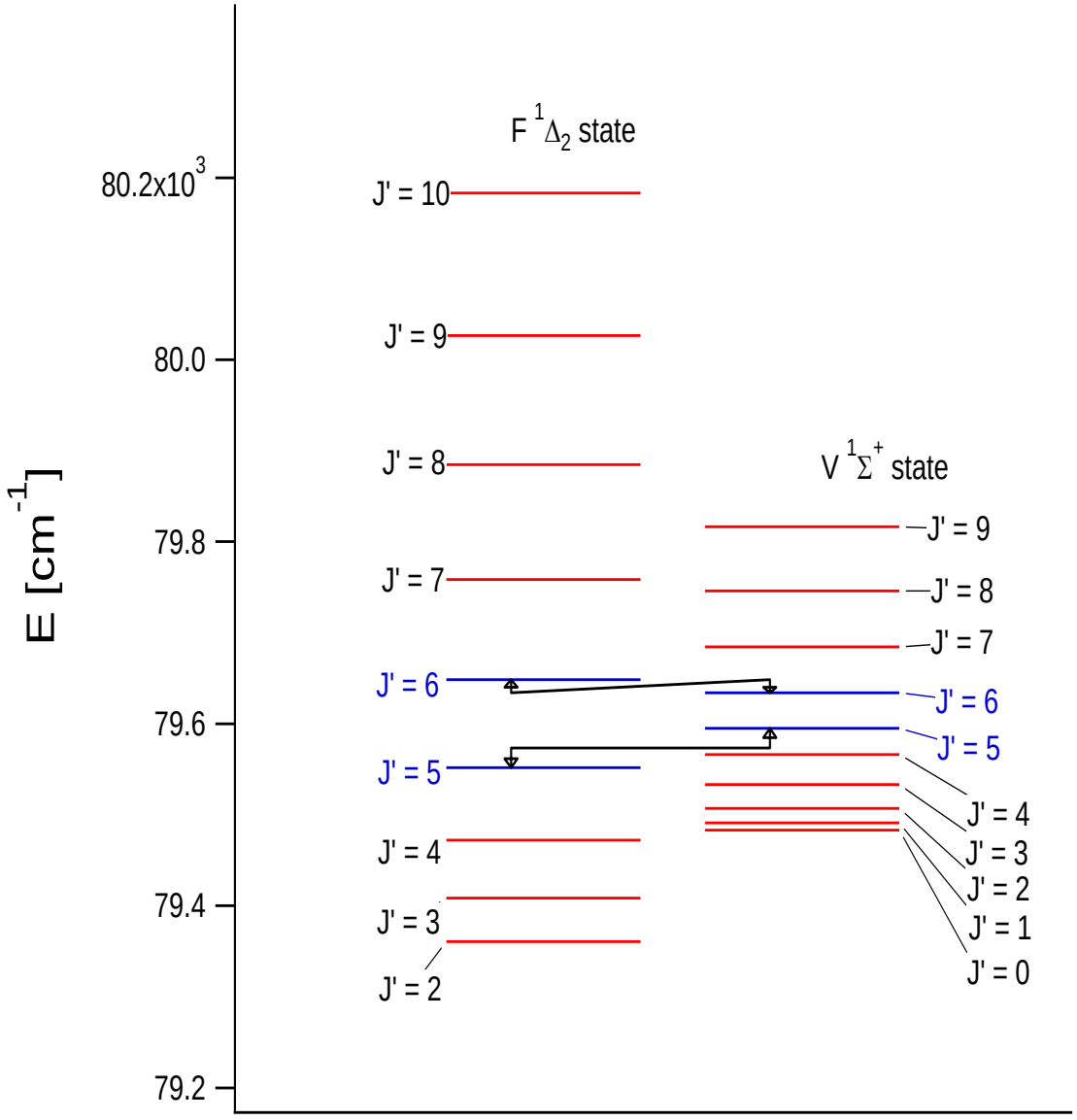

Figure 3-1 Calculated energy levels for the F and V states. From the calculated energy levels it is clear that some kind of state-state interaction could occur, i.e. the J‘ = 5 peak position of the F state and J‘ = 6 peak position of the V state could be observed at a lower wavenumber and the J‘ = 6 peak position of the F state and the J‘ = 5 peak of the V state could be observed at a higher wavenumber.

a)

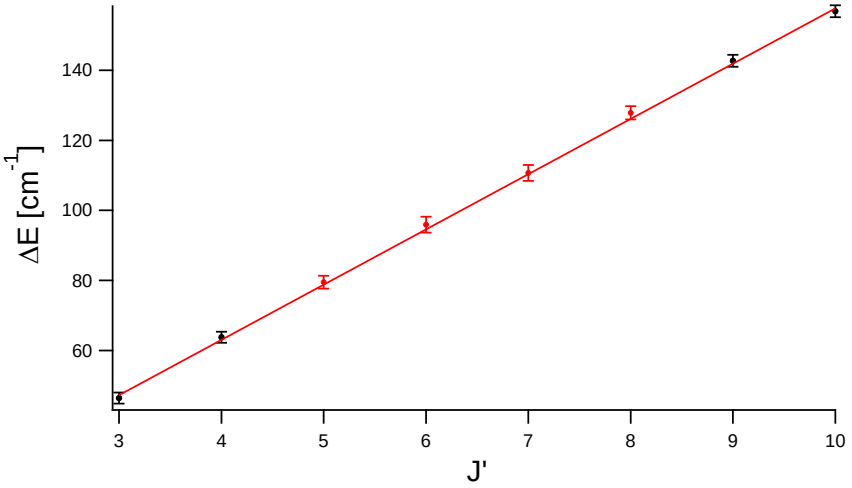

b)

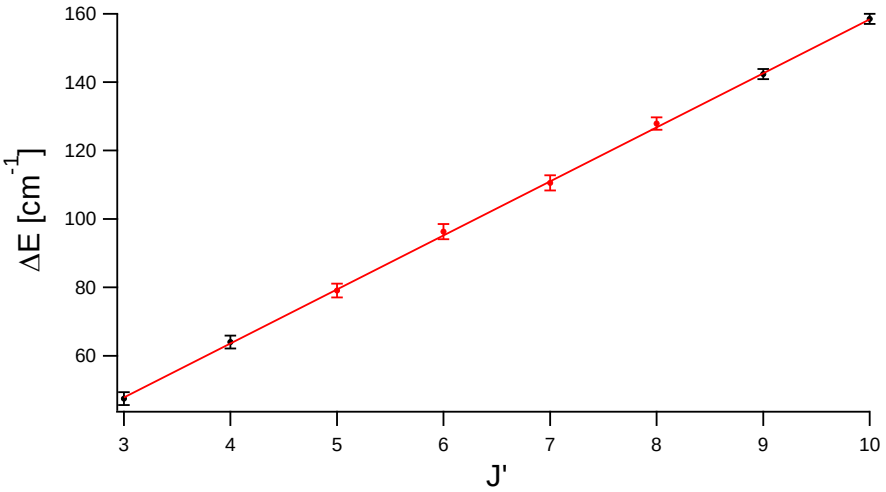

Figure 3-2 Energy level spacing ($\Delta E_{J',J'-1}$ = E(J‘)-E(J‘-1)) as a function of rotational levels, J‘ in the a) 79 isotopomer and the b) 81 isotopomer within the F state. The expected shift of peaks is surprisingly not observed.

3.2.2 The V $^1\Sigma^+$ (m+7) ion-pair state

The line shift analysis for the V state was performed in the same manner as for the F state. The results are quite curious.

It seems that, even though the F state exhibits no definite line shift characteristics, the V state seems to be surpassingly perturbed (Figure 3.3). Both the J‘ = 5,6 ΔE‘s appear lower than is to be expected, as well as for the J‘ = 7 ΔE‘s, whereas the values for the J‘ = 3 and J‘ = 2 ΔE‘s appear slighty higher. From these data one could argue that while the F state exhibits no characteristic line shift interaction, the V state is severely perturbed.

a)

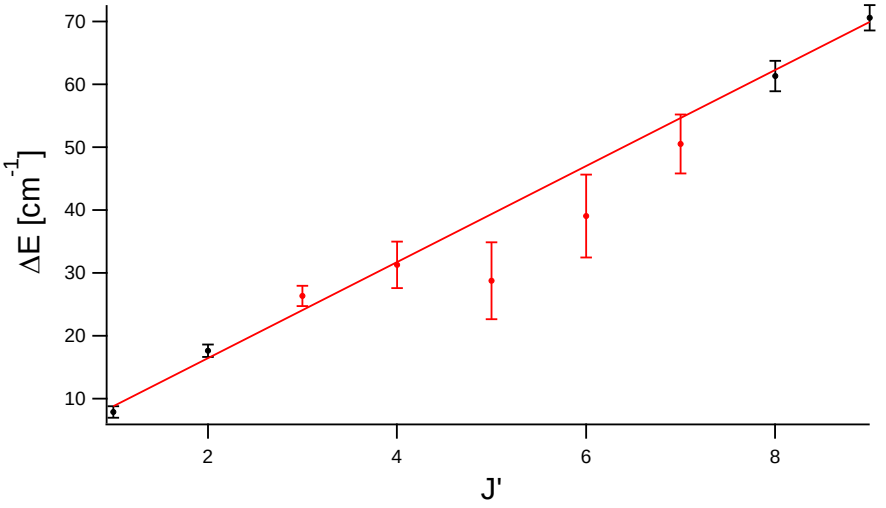

b)

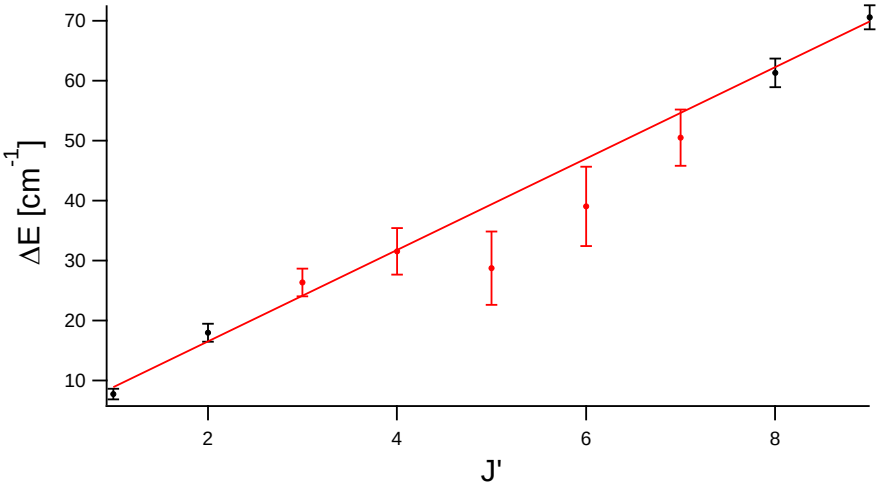

Figure 3-3 Energy level spacing as a function of rotational levels, J‘ in the a) 79 isotopomer and the b) 81 isotopomer within the V state. The results are not what was to be expected and hint at enormous line shifts within the V state; a trait not shared with the F state.

The smallest placing between rotational energy levels of the F state and the V state for the same J‘ quantum numbers is found to be between J‘ = 5 and 6 (Table 3.15). First order unshifted energy levels were derived both for the F and V (m+7) states in the line shift analysis, $E_1^0(J')$ and $E_2^0(J')$ respectively. From these energy values on top of the energies of the perturbed energy levels, E(J‘), interaction strength, W_{12}, could be calculated[30-32] as a function of J‘ from

$$W_{12} = \left[\frac{1}{4}\left\{\left(2\left(\langle\frac{1}{2}\left(E_1^0(J')+E_2^0(J')\right)\rangle - E_1(J')\right)\right)^2 - \left(E_1^0(J')-E_2^0\right)^2\right\}\right]^{\frac{1}{2}} \quad (5)$$

Table 3-15 Energy difference between the calculated energy levels of the $F^1\Delta_2$ (1,0) state and the $V^1\Sigma^+$ (m+7) state for each rotational quantum number J‘.

	$\Delta E = E(F^1\Delta_2(1,0)) - E(V^1\Sigma^+(m+7))\ [cm^{-1}]$	
J‘	*79 isotopomer*	*81 isotopomer*
2	-146.2 ± 0.8	-145.8 ± 1.1
3	-124.5 ± 1.5	-124.3 ± 1.2
4	-94 ± 4	-95 ± 2
5	-43 ± 5	-44 ± 2
6	14 ± 4	14 ± 2
7	74 ± 2	74 ± 2
8	139 ± 2	138.5 ± 1.4
9	210 ± 2	210 ± 2

3.3 Ion-pair signal intensity ratio analysis (IPSIRA)

3.3.1 The F $^1\Delta_2$ (1,0) Rydberg state

The interaction strength parameter, W_{12}‘ was derived from the expression

$$W_{12}(J') = W'_{12}\sqrt{J'(J'+1)} \quad (6)$$

which holds for a heterogeneous interaction ($\Delta\Omega \neq 0$) as is the case between the F and V states. The fractional contributions to the state mixing (c_1^2 for the $F^1\Delta_2$ Rydberg state and c_2^2 for the $V^1\Sigma^+$ ion-pair state) are now easily derived from W_{12} and the energy difference $\Delta E_{J'} = E_1(J') - E_2(J')$ as

$$c_1^2 = \frac{1}{2} + \frac{\sqrt{(\Delta E_{J'})^2 - 4(W_{12})^2}}{2|\Delta E_{J'}|};\ c_2^2 = 1 - c_1^2 \quad (7)$$

An expression for $I(Br^+)/I(HBr^+)$, (in this particular example we make the assumption that the ionization channels for HCl and HBr respectively are equivalent) as a function of the mixing fraction, c_2^2, based on ionization processes following resonance excitation, has been derived as

$$\frac{I(Br^+)}{I(HBr^+)} = \frac{\alpha[\gamma + c_2^2(1-\gamma)]}{(1-c_2^2)};\ I(Br^+) = \alpha_2 c_2^2 + \beta_1 c_1^2;\ I(HBr^+) = \alpha_1 c_1^2 + \beta_2 c_2^2 \quad (8)$$

where α ($=\alpha_2/\alpha_1$) measures the relative rate of the two major / characteristic ionization channels, i.e. for the Br^+ formation for excitation from the diabatic ion-pair state (α_2) to the HBr^+ formation from the diabatic Rydberg state (α_1). γ ($=\beta_1/\alpha_2$) represents the rate of Br^+ formation via the diabatic Rydberg state (β_1; referred to as the „dissociative channel“ in reference 31) to that of its formation from the diabatic ion-pair state (α_2), which is one of the major / characteristic ionization channels. Hence γ is a relative measure of the importance of the „dissociative channel“. Expression (8) allows the relative ion signals as a function of J‘ to be fitted to derive α and γ (Table 3.16 and Figure 3.4).

Table 3-16 Parameter values, relevant to state mixing derived from peak shifts and intensity ratios ($I(^iBr^+)/I(H^iBr^+)$) as a function of J‘.

	$F^1\Delta_2$ (1,0)	
Isotopomers	$H^{79}Br$	$H^{81}Br$
J‘ closest resonance (J'_{res})	6	6
$\lvert\Delta E(J'_{res})\rvert$ [cm^{-1}]	14 ± 4	14 ± 2
W_{12} [cm^{-1}]	7 ± 2	7 ± 1
W_{12}‘ [cm^{-1}]	1.11 ± 0.10	1.09 ± 0.05
c_1^2 (c_2^2)	0.50 ± 0.10 (0.50 ± 0.10)	0.50 ± 0.09 (0.50 ± 0.09)
γ	0.557 ± 0.005	0.767 ± 0.005
α	0.349 ± 0.005	0.181 ± 0.005

Integration of peaks was carried out in IGOR Pro 6th edition undir the „Multipeak fitting“ procedure inscribed in the program. From the Multipeak fitting procedure both integration of peaks and bandwidth measurements were obtained along with uncertainties.

From the calculated γ ($=\beta_1/\alpha_2$) values shown in Table 3.16 it can be seen that the importance of the dissociative channel, γ, is a lot more significant than for HCl[31,32]. Even more noteworthy is the value of α ($=\alpha_2/\alpha_1$), the relative rate of the Br^+ formation via ion-pair state to the HBr^+ formation via the Rydberg state. While the Rydberg state does actually hold dominion over its HBr^+ formation channel, the dissociative channel α_2, actually dominates the Br^+ formation channel as well over the V state. We can therefore conclude that the V state in this example serves mainly as a gateway state to a repulsive state.

When the two isotopomers are compared, the α and γ values differ quite a bit but in accordance with Figure 3.4 this difference can be explained. The α constant is a scaling factor and accounts for the height of the background of the respective columns in Figure 3.4. The γ factor accounts however for the ratio between the intensities of the resonance transitions and the background intensities. Now, since the ion-pair ratio is in most cases lower for the 81 isotopomer, the difference between the calculated α and γ values are obtained (lower height of background accounts for a lower α value and axiomatically the higher value of γ while the lower intensity in the J‘ = 6 column also contributes to the higher value of γ).

a)

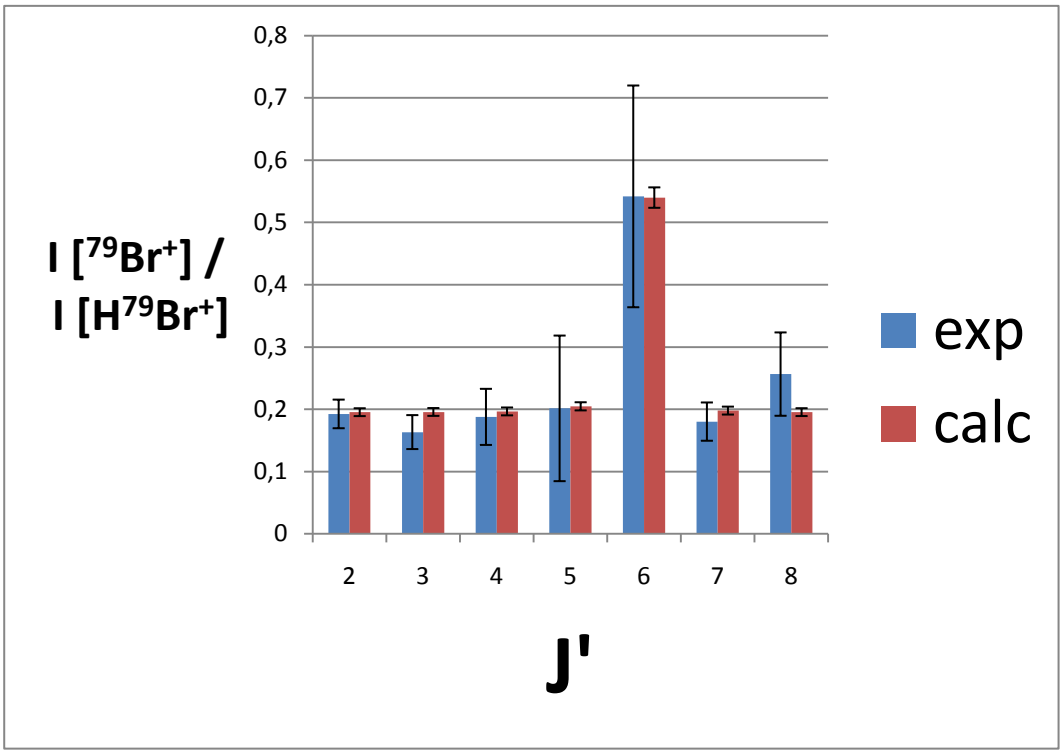

b)

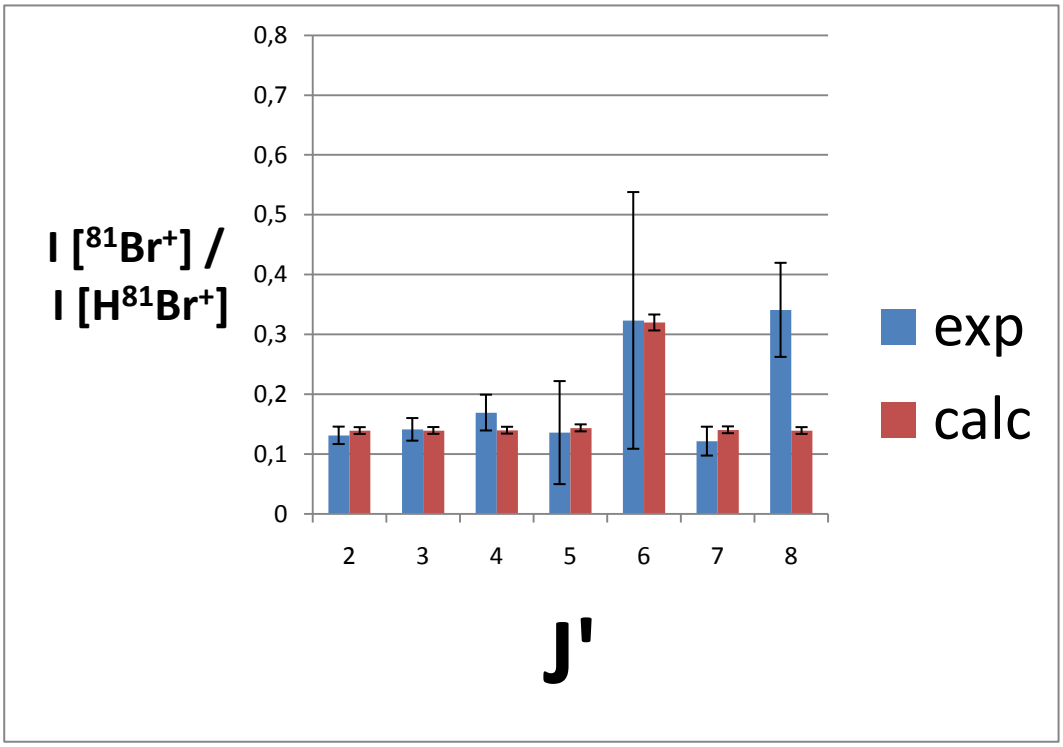

Figure 3-4 Relative ion signal intensities, $I(^{i}Br^{+})/I(H^{i}Br^{+})$ a) i = 79 and b) i = 81 vs. J‘ derived from Q rotational lines of REMPI spectra due to resonance transitions between the F and V states (blue columns) and simulations, assuming J‘ level-to-level interactions between the F state and V state (red columns).

3.3.2 The H $^1\Sigma^+$ (0,0) Rydberg state

The H state is quite unorthodox in its own way. By observing the calculated energy levels for the H and V states it is unraveled that the H state is „clenched“ between the $V^1\Sigma^+$ (m+7) and the $V^1\Sigma^+$ (m+8) states (Figure 3.5 and Table 3.17).

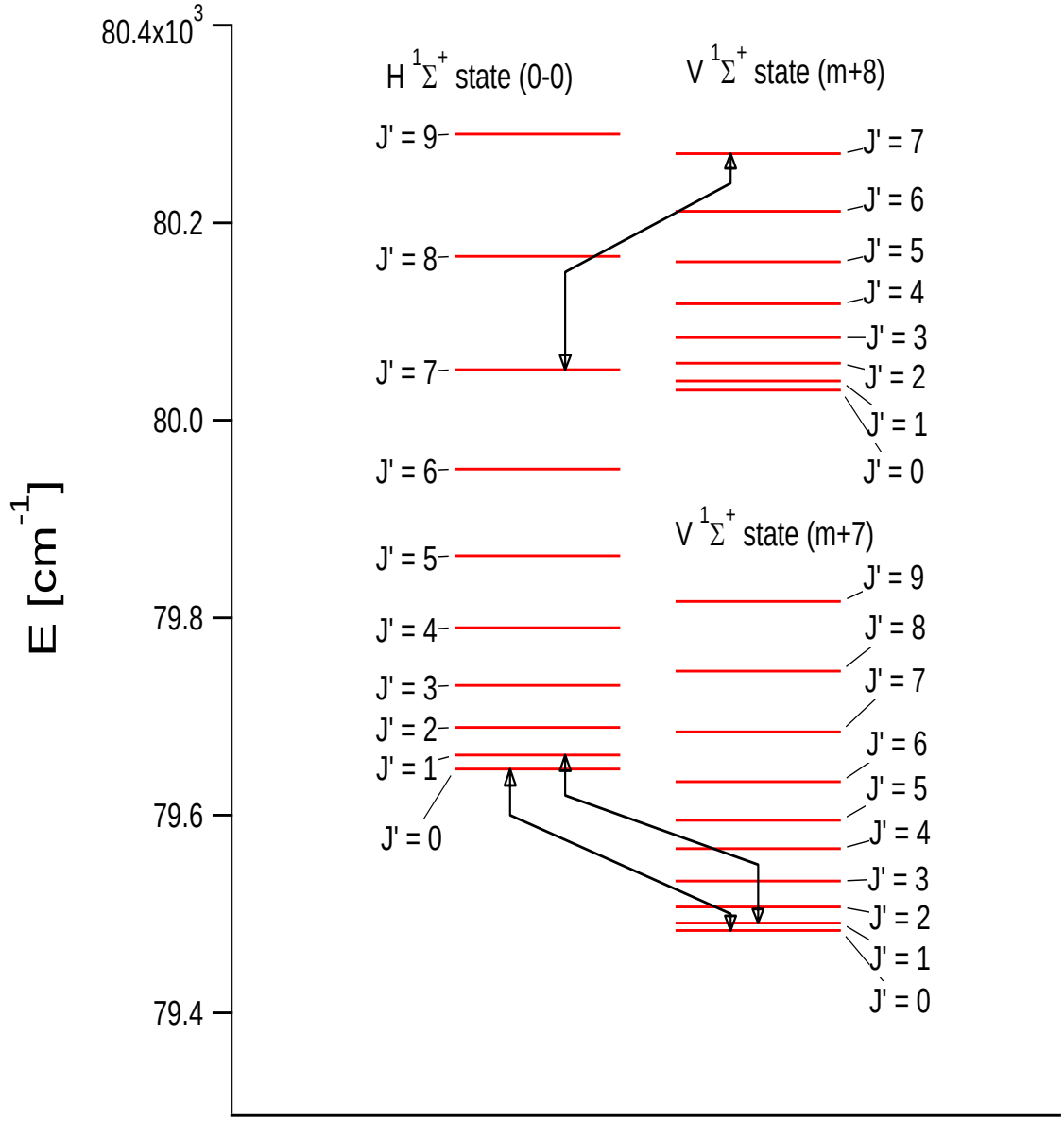

Figure 3-5 Calculated energy states for the H and V states. The schematic shows how the calculated energy levels of the H state are „clenched“ between the two V states and how interactions are likely to occur between the energy states.

Table 3-17 Energy difference between the calculated energy levels (see expression 3) of the $H^1\Sigma^+$ (0,0) state and the a) $V^1\Sigma^+$ (m+7) state for each rotational quantum number J‘ and b) the $V^1\Sigma^+$ (m+8) state for each rotational quantum number J‘. The values for the V (m+8) state were made available by associate J. Long (work unpublished).

a)

	$\Delta E = E(H^1\Sigma^+ (0,0)) - E(V^1\Sigma^+ (m+7))\ [cm^{-1}]$	
J‘	*79 isotopomer*	*81 isotopomer*
0	163.8 ± 1.0	164.0 ± 1.0
1	169.9 ± 0.9	170.5 ± 0.8
2	181.9 ± 0.9	182.6 ± 0.9
3	198.2 ± 1.5	198.8 ± 1.1
4	223.7 ± 3.5	223.6 ± 3.5
5	268.0 ± 5.1	267.8 ± 5.1
6	316.7 ± 4.3	316.5 ± 4.3
7	366.8 ± 2.1	366.8 ± 2.1
8	420.1 ± 1.4	419.9 ± 1.5
9	473.5 ± 1.9	473.3 ± 1.9

b)

	$\Delta E = E(H^1\Sigma^+ (0,0)) - E(V^1\Sigma^+ (m+8))\ [cm^{-1}]$	
J‘	*79 isotopomer*	*81 isotopomer*
0	-383.5 ± 0.7	-383.5 ± 0.7
1	-379.0 ± 0.6	-379.0 ± 0.6
2	-369.0 ± 0.5	-369.0 ± 0.5
3	-352.4 ± 0.5	-352.4 ± 0.5
4	-328.0 ± 0.2	-328.0 ± 0.2
5	-297.6 ± 0.5	-297.6 ± 0.5
6	-261.1 ± 0.7	-261.1 ± 0.7
7	-218.6 ± 0.5	-218.6 ± 0.5

This would mean that interaction strengths with the V state could be most prominent at the quantum rotational numbers J‘ = 0,1 and J‘ = 7,8,9 (where the energy difference is lowest between the H state and the V states). However since there are no lines visible above J‘ = 7 for the V (m+8) state, calculated values originated from the V (m+8) state will not extend to the J‘ = 8,9 lines of simulations.

Assuming, to a first approximation, that the ion intensity ratio is a sum of contributions due to interactions from the V (m+7) and V (m+8) states for common α and γ parameters, $I(^iBr^+)/I(H^iBr^+)$ can be expressed as

$$\frac{I(Br^+)}{I(HBr^+)} = \alpha\left\{\frac{\left[\gamma + c_{2,m+7}^2(1-\gamma)\right]}{\left(1 - c_{2,m+7}^2\right)} + \frac{\left[\gamma + c_{2,m+8}^2(1-\gamma)\right]}{\left(1 - c_{2,m+8}^2\right)}\right\} \quad (9)$$

where $c^2_{2,m+7}$ and $c^2_{2,m+8}$ are the fractional mixing contributions for V (m+7) and V (m+8) respectively.

Table 3-18 Parameter values, relevant to state mixing of the H state and the V (m+7) and V (m+8) states respectively, derived from peak shifts and intensity ratios ($I(^iBr^+)/I(H^iBr^+)$) as a function of J‘. The interaction strength, W_{12}, is assumed to be approximately half the energy difference between resonance states, $|\Delta E(J'_{res})|$, with a large uncertainty factor.

	$H^1\Sigma^+$; $v'= 0$	
	79 isotopomer – (m+7) / (m+8)	*81 isotopomer – (m+7) / (m+8)*
J'_{res}	0 / 7	0 / 7
$\|\Delta E(J'_{res})\|$ [cm^{-1}]	163.8 ± 1.0 / -218.6 ± 0.5	164.0 ± 1.0 / -218.6 ± 0.5
W_{12} [cm^{-1}]	81 ± 2 / 109 ± 5	81 ± 2 / 109 ± 5
c_1^2 (c_2^2)	0.57 (0.43) ± 0.10 / 0.91 (0.09) ± 0.01	0.58 (0.42) ± 0.10 / 0.91 (0.09) ± 0.01
γ	0.56 ± 0.01	0.55 ± 0.01
α	0.72 ± 0.01	0.75 ± 0.01

The α (=α_2/α_1) values in Table 3.18 reveal that the Br^+ formation via the ion-pair states (α_2) is dominated by the HBr^+ formation via the Rydberg state (α_1). According to the γ (=β_1/α_2) values, the dissociative channel (β_1) is dominated by the ion-pair state, i.e. $\gamma \approx 0.5$. This suggests prominent off-resonance interaction, but not near-resonance interaction, like between the F state and V (m+7) state.

When relative ion intensities are compared with calculated values (Figure 3.6) it is clear that perturbations are more prominent at J‘ = 0,1 of the H state, as to be expected. According to calculated values, however, an increase is expected at J‘ = 7, which is not experimentally observed.

Calculated and experimental values do follow a similar trend and uncertainty is at its highest within the calculated and experimental results for the lowest and highest rotational quantum numbers. Due to the unclear assignment of the interaction strengths, W_{12}, the largest uncertainties of the calculated results are at the highest rotational quantum number.

a)

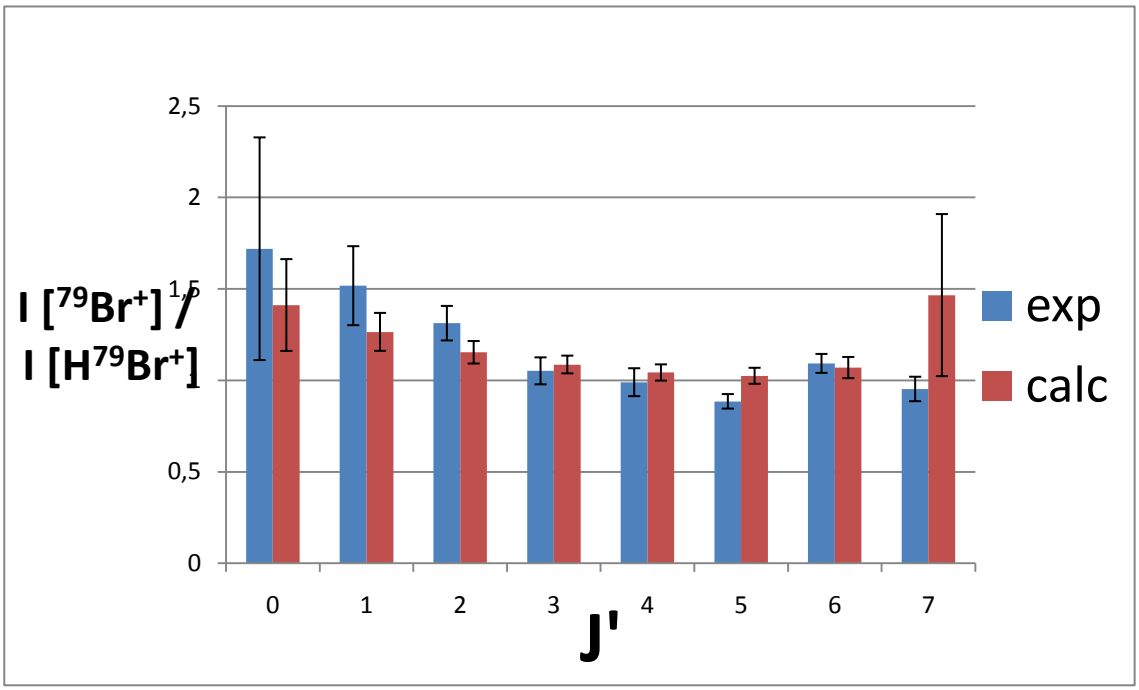

b)

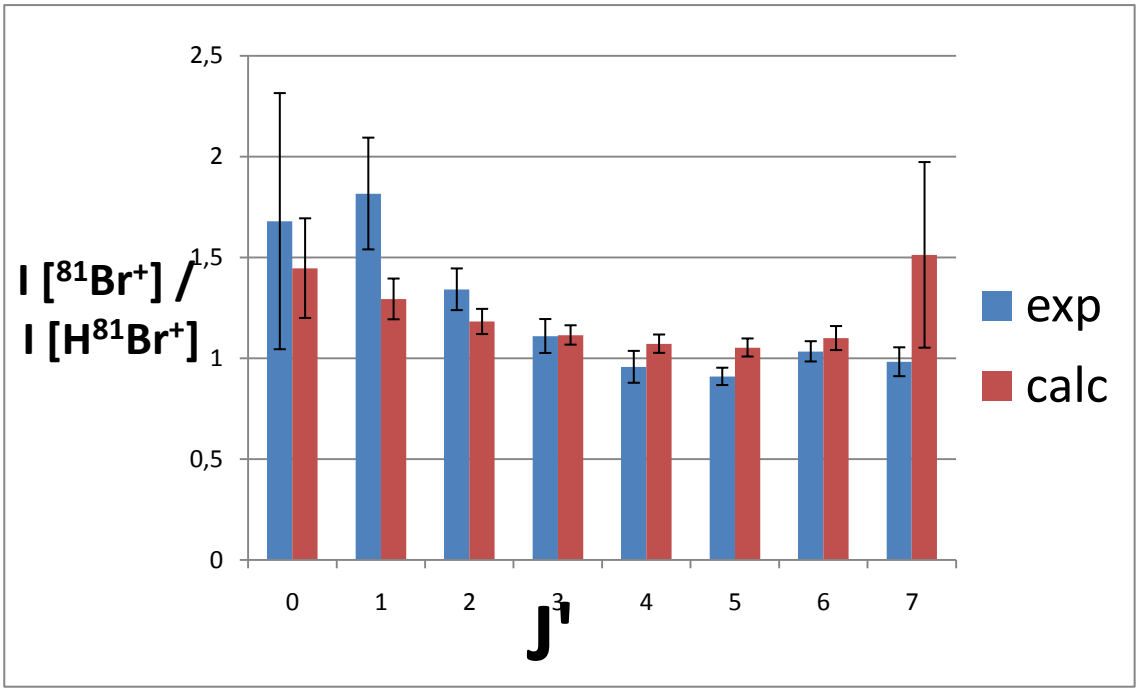

Figure 3-6 Relative ion signal intensities, $I(^{i}Br^{+})/I(H^{i}Br^{+})$ a) i = 79 and b) i = 81 vs. J‘ derived from Q rotational lines of REMPI spectra due to off-resonance transitions between the H state and V states (blue columns) and simulations, assuming J‘ level-to-level interactions between the H state and V states (red column).

3.4 Bandwidth analysis

Classically, bandwidth is defined as the full width at half maximum (FWHM) of a peak. In this study, peaks represent energy states and the bandwidth inversely represents the lifetime of each energy state via the expression

$$\tau\ [ps] = \frac{5.3}{BW\ [cm^{-1}]} \quad (10)$$

where τ is the lifetime of the state in ps and BW is the bandwidth of the correspond peak in cm^{-1}. Higher bandwidth (broader peaks) should therefore be representative of short lifetimes of states. However expression (6) can only provide us with a lower limit of the lifetime for the sharpest peaks because the spectra are recorded in 0.1 cm^{-1} wavenumber steps. Therefore, it is likely that the actual height of the observed peaks could be substantially higher but due to the detection limit of the predetermined wavenumber steps, the actual height of the peaks is not observed and henceforth a lower limit is set for the lifetime of the associated energy states. By that virtue alone we can also conclude that larger bandwidths could therefore in general provide a more accurate result for the lifetimes of energy states.

3.4.1 The F $^1\Delta_2$ (1,0) Rydberg state

The ion-intensity analysis concluded that there were near-resonance interactions between the F state and the V state in the vicinity of the J‘ = 6 rotational quantum state. A rise in the bandwidth around that same rotational quantum state should therefore unambiguously conclude an established perturbation between the F state and the V state.

By observing the bandwidths of the H^iBr^+ signals (the ion formation channel via the Rydberg state) within the F state, the lifetime of the quantum rotational states within the F state can be calculated and interaction characteristics observed with a drop in the lifetime of the J‘ = 6 rotational quantum state (Table 3.19 and Figure 3.7). What is surprising though is that the largest bandwidth is observed at J‘ = 5 but not J‘ = 6, but a trend does exist where bandwidth increases around J‘ = 5 (where J‘ = 6 is included).

Table 3-19 Bandwidths and corresponding lifetimes of the rotational quantum states, J‘, within the $F^1\Delta_2$ state. A slight increase in bandwidth is observed around J‘ = 5 as well as a corresponding decrease in lifetime indicative of interaction between the $F^1\Delta_2$ state and the $V^1\Sigma^+$ (m+7) state.

	BW [cm^{-1}]		*τ [ps] (lower limit)*	
J‘	*79 isotopomer*	*81 isotopomer*	*79 isotopomer*	*81 isotopomer*
2	0.78 ± 0.02	0.82 ± 0.01	6.81 ± 0.15	6.45 ± 0.12
3	0.80 ± 0.02	0.80 ± 0.02	6.60 ± 0.18	6.59 ± 0.14
4	0.98 ± 0.04	1.00 ± 0.03	5.41 ± 0.24	5.28 ± 0.17
5	1.22 ± 0.16	1.32 ± 0.11	4.34 ± 0.56	4.01 ± 0.33
6	0.95 ± 0.11	0.93 ± 0.08	5.59 ± 0.67	5.72 ± 0.47
7	0.79 ± 0.10	0.84 ± 0.07	6.75 ± 0.88	6.33 ± 0.53
8	0.77 ± 0.41	0.99 ± 0.26	6.87 ± 3.62	5.38 ± 1.40
9	0.77 ± 0.31	0.97 ± 0.60	6.86 ± 2.77	5.45 ± 3.38

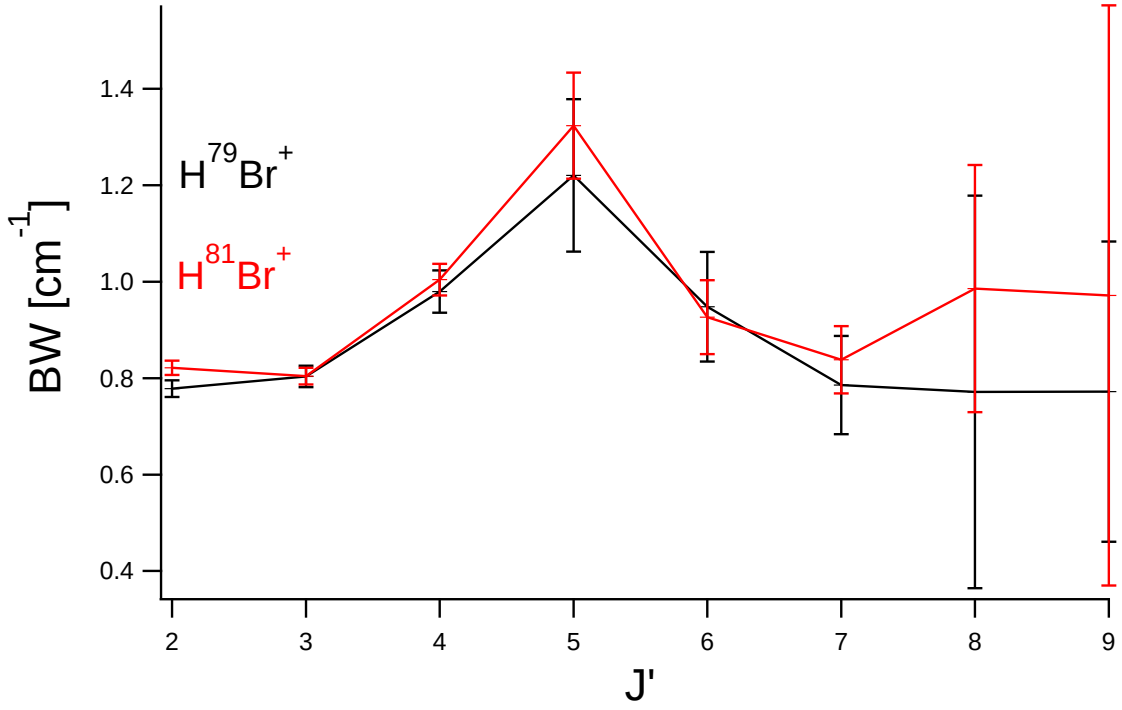

Figure 3-7 Bandwidth as a function of rotational quantum numbers, J‘ for the $F^1\Delta_2$ (1,0) state. A significant increase is observed in bandwidth which is indicative of interaction with the $V^1\Sigma^+$ (m+7) state.

3.4.2 The V $^1\Sigma^+$ (m+7) ion-pair state

Although the line shift analysis of the V state seemed very unreliable at first, it did show distinctive perturbation effects. IPSIRA then revealed that the V state was fighting a losing battle against the diabatic Rydberg state for ionization channeling.

The bandwidth analysis, however, reveals a major increase in bandwidth as well as reduced lifetime of the J‘ = 5 and J‘ = 6 rotational quantum states (Table 3.19 and Figure 3.8). This fact reciprocates with the calculated parameters α and γ, and for the first time it is shown that a trend exists between bandwidth and relative ion signal intensities.

Table 3-20 Bandwidths and corresponding lifetimes of the rotational quantum states, J‘, within the $V^1\Sigma^+$ (m+7) state. A gargantuan increase in bandwidth is observed at J‘ = 4-6 and a corresponding decrease in lifetime as well is indicative of interaction between the $F^1\Delta_2$ state and the $V^1\Sigma^+$ (m+7) state.

	BW [cm^{-1}]			*τ [ps] (lower limit)*		
J‘	H^+	$^{79}Br^+$	$^{81}Br^+$	H^+	$^{79}Br^+$	$^{81}Br^+$
0	2.40 ± 0.09	1.71 ± 0.10	2.02 ± 0.12	2.21 ± 0.08	3.10 ± 0.18	2.63 ± 0.15
1	2.34 ± 0.04	2.05 ± 0.06	2.15 ± 0.06	2.26 ± 0.04	2.58 ± 0.07	2.46 ± 0.06
2	2.82 ± 0.05	2.43 ± 0.07	2.45 ± 0.06	1.88 ± 0.03	2.18 ± 0.06	2.16 ± 0.06
3	3.23 ± 0.13	2.60 ± 0.21	2.73 ± 0.20	1.64 ± 0.06	2.03 ± 0.16	1.94 ± 0.14
4	10.2 ± 0.30	9 ± 2	9.0 ± 1.2	0.52 ± 0.01	0.57 ± 0.10	0.59 ± 0.08
5	20 ± 5	30 ± 10	30 ± 10	0.26 ± 0.07	0.18 ± 0.06	0.18 ± 0.06
6	19 ± 2	11.9 ± 1.1	15 ± 5	0.28 ± 0.03	0.45 ± 0.04	0.37 ± 0.12
7	6.10 ± 0.12	3.1 ± 1.7	3.9 ± 1.3	0.87 ± 0.02	1.72 ± 0.94	1.36 ± 0.46
8	4.51 ± 0.11	6.73 ± 0.50	4.75 ± 0.35	1.17 ± 0.03	0.79 ± 0.06	1.12 ± 0.08
9	3.58 ± 0.16	2.76 ± 0.52	2.87 ± 0.56	1.48 ± 0.06	1.92 ± 0.36	1.85 ± 0.36

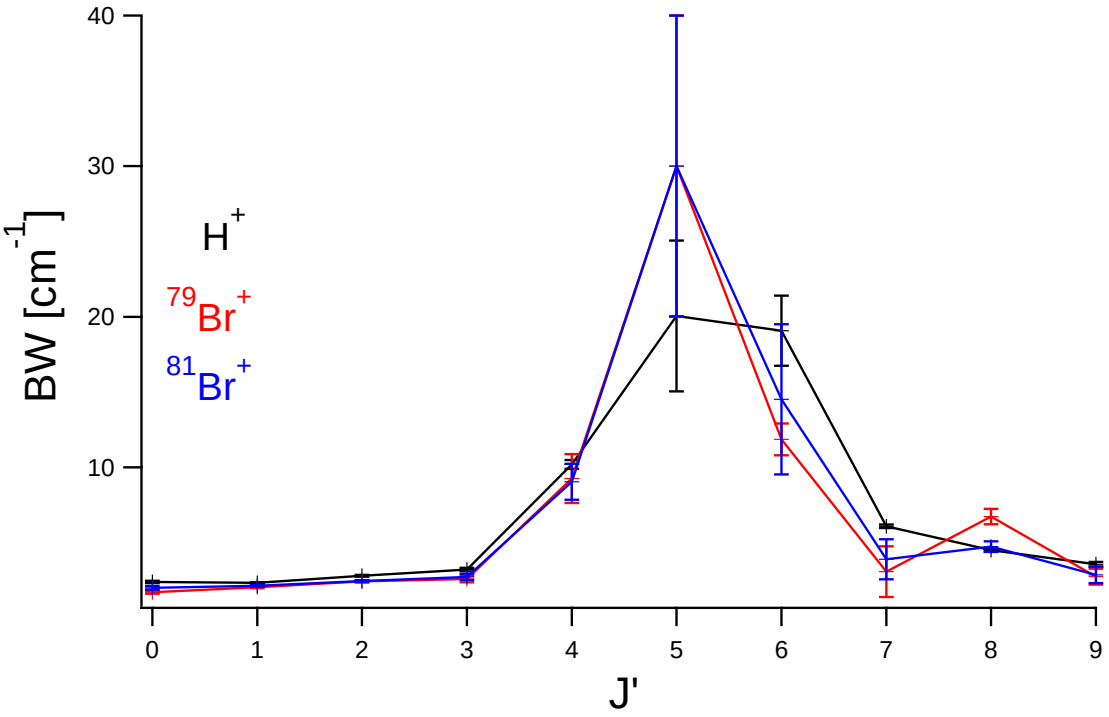

Figure 3-8 Bandwidth of H^+ signals (black), $^{79}Br^+$ signals (red) and $^{81}Br^+$ signals (blue) as a function of rotational quantum numbers, J‘ for the $V^1\Sigma^+$ (m+7) state. A clear increase is observed in bandwidth which is indicative of near-resonance interaction with the $F^1\Delta_2$ (1,0) state.

3.4.3 The H $^1\Sigma^+$ (0,0) Rydberg state

Bandwidth analysis was performed for the H state to inspect whether a trend could be found between the bandwidths and the ion signal intensities as was the case for the F state

and V state. IPSIRA revealed that the H state was perturbed by both the V (m+7) and V (m+8) states but the uncertainty factor of the higher rotational quantum numbers, J‘ = 8,9 was extremely high in the experimental part and non-existent in the simulative part due to the fact that those lines are not visible for the V(m+8) state.

It is therefore expected that the bandwidths should be greatest at the lowest and highest rotational quantum numbers, J‘ = 1,2 and 8,9, but with high uncertainty.

Table 3-21 Bandwidths of the $^{i}Br^{+}$ ion signals and corresponding lifetimes of their respective rotational quantum states. An increase in lifetime is observed for J‘ = 4 signifying that perturbation is present from the V states.

	BW [cm^{-1}]		*τ [ps] (lower limit)*	
J‘	*79 isotopomer*	*81 isotopomer*	*79 isotopomer*	*81 isotopomer*
0	1.31 ± 0.21	1.19 ± 0.20	4.05 ± 0.66	4.45 ± 0.74
1	1.13 ± 0.07	1.17 ± 0.08	4.67 ± 0.30	4.51 ± 0.29
2	1.06 ± 0.04	1.07 ± 0.04	5.00 ± 0.18	4.96 ± 0.18
3	1.03 ± 0.04	1.10 ± 0.04	5.16 ± 0.20	4.81 ± 0.19
4	0.89 ± 0.04	0.88 ± 0.04	5.95 ± 0.27	6.00 ± 0.28
5	1.14 ± 0.03	0.88 ± 0.04	4.64 ± 0.12	6.00 ± 0.30
6	1.16 ± 0.03	0.92 ± 0.05	4.56 ± 0.11	5.77 ± 0.32
7	1.10 ± 0.04	1.11 ± 0.05	4.81 ± 0.18	4.76 ± 0.19
8	1.22 ± 0.09	1.21 ± 0.10	4.35 ± 0.33	4.38 ± 0.35
9	0.93 ± 0.24	1.14 ± 0.28	5.7 ± 1.5	4.7 ± 1.1

Table 3-22 Bandwidths of the $H^{i}Br^{+}$ ion signals and corresponding lifetimes of their respective rotational quantum states. An increase in lifetime is observed for J‘ = 4 signifying that perturbation is present from the V states.

	BW [cm^{-1}]		*τ [ps] (lower limit)*	
J‘	*79 isotopomer*	*81 isotopomer*	*79 isotopomer*	*81 isotopomer*
0	1.21 ± 0.29	1.07 ± 0.28	4.4 ± 1.1	4.9 ± 1.3
1	1.14 ± 0.10	1.00 ± 0.11	4.66 ± 0.42	5.31 ± 0.56
2	1.10 ± 0.05	1.12 ± 0.06	4.82 ± 0.22	4.72 ± 0.23
3	1.02 ± 0.04	1.05 ± 0.05	5.18 ± 0.20	5.06 ± 0.23
4	0.83 ± 0.03	0.87 ± 0.04	6.40 ± 0.27	6.09 ± 0.28
5	1.11 ± 0.03	1.09 ± 0.03	4.76 ± 0.12	4.88 ± 0.13
6	1.09 ± 0.03	1.07 ± 0.03	4.85 ± 0.14	4.95 ± 0.14
7	1.07 ± 0.05	1.02 ± 0.04	4.93 ± 0.21	5.18 ± 0.22
8	1.24 ± 0.14	1.01 ± 0.11	4.26 ± 0.46	5.25 ± 0.56
9	0.57 ± 0.22	1.37 ± 0.74	9.3 ± 3.9	3.9 ± 2.1

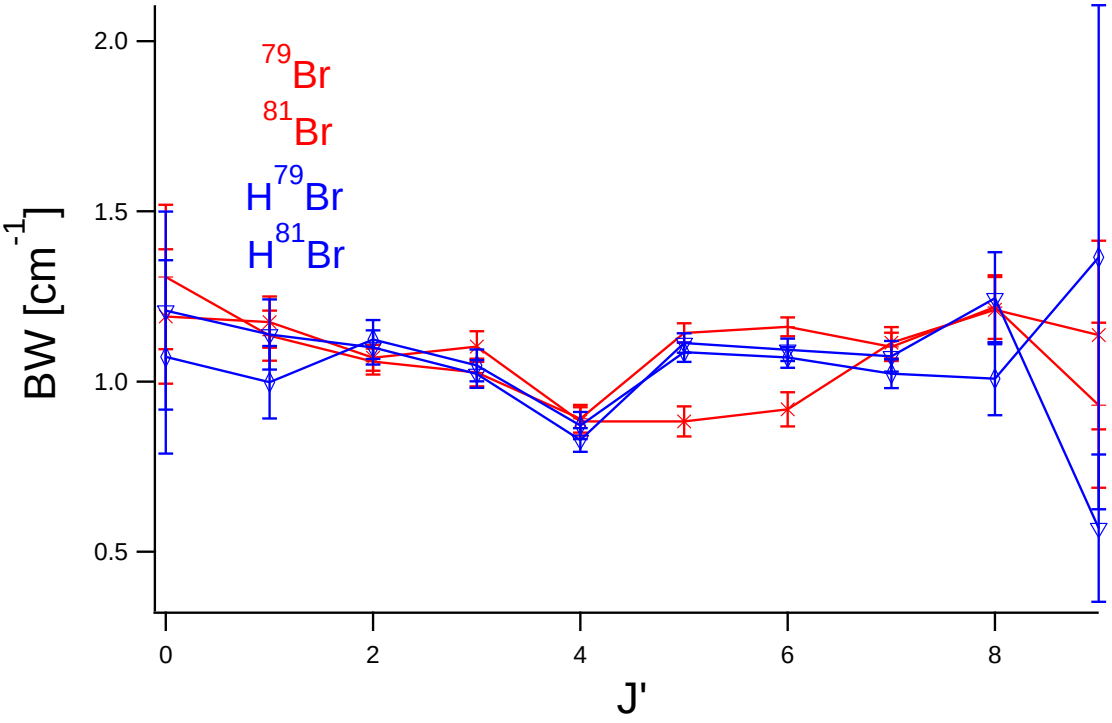

Figure 3-9 Bandwidth of the ion signals, $^{i}Br^{+}$ (red) and $H^{i}Br^{+}$ (blue) as a function of the the rotational quantum numbers, J‘. Observed is a slight decrease in the bandwidths of all ion signals from J‘ = 0-4 and a slight increase in bandwidths of all ion signals from J‘ = 4-8. Uncertainty too high for clear evaluation in J‘ = 9.

From Table 3.18 and Figure 3.9 it can be concluded that there is a decrease in bandwidth from J‘ = 0-4 and an increase in bandwidth from J‘ = 4-8. This trend signifies a decreasing interaction between the H state and the V (m+7) state from J‘ = 0-4 and an increasing interaction between the H state and the V (m+8) state from J‘ = 4-8. Values in Table 3.17 could have predicted these results (as well as Figure 3.5) since the energy difference between the calculated energy levels of the H state and the V (m+7) state was minimal at the lowest rotational quantum numbers while the energy difference between the H state and the V (m+8) state was minimal at the highest rotational quantum numbers.

Thus it has been shown that the bandwidth analysis unqueastionably provides both qualitative information (by confirming predicted state perturbations) and quantitative information (calculated life times of states). This makes bandwidth analysis an applicable tool in future state-state mixing calculations.

3.5 Atomic lines

In the region 78960 – 79820 cm^{-1} two atomic lines are observed at 79181.9 cm^{-1} and 79692.9 cm^{-1} respectively. Both of the atomic lines lie very close to the calculated energy levels of the $f^{3}\Delta_{1}$ state and the $F^{1}\Delta_{2}$ state respectively (Table 3.23).

Table 3-23 Calculated quantum rotational energy levels of the f $^3\Delta_1$ and $F^1\Delta_2$ states respectively in the closest vicinity of observed positions of atomic lines.

	J'	*Energy level [cm^{-1}]*	*Atomic line [cm^{-1}]*
$f^3\Delta_1$	4	79187.0	79181.9
$F^1\Delta_2$	6-7	79645.1 – 79755.6	79692.9

From the values in Table 3.23 a couple of suggestive conclusions can be drawn.

- 1; Vicinity to a repulsive dissociative state could account for the low intensity of the the $f^3\Delta_1$ Rydberg state and absolutely no clear intensity of any $^iBr^+$ signal in its vicinity.

- 2; Vicinity to a repulsive dissociative state could also account for some of the perturbation effects reveiled in the line shift analysis of the V state (between J' = 6 and 7).

4 Conclusion

REMPI-TOF has been used to measure the two-photon absorption spectrum of HBr between 78960 – 79820 cm^{-1}. Over this energy range the excited energy states $f^3\Delta_1$, $F^1\Delta_2$, $V^1\Sigma^+$ (m+7) and $H^1\Sigma^+$ were measured and analyzed thouroughly.

Assignments of peaks and energy levels were made in the $f^3\Delta_1$, $F^1\Delta_2$ and $V^1\Sigma^+$ (m+7) states that have never been assigned before and line shift analysis as well as ion-pair signal intensity ratio analysis (IPSIRA) were used to measure the perturbation effects due to resonance state mixing between the F and V state. IPSIRA was used to determine perturbation effects in the H state between the V(m+7) and V(m+8) states.

Last but not least quantitative and qualitative bandwidth analysis was successfully used to calculate lower-limits for the lifetimes of quantum rotational states and determine similar trends in the ion-pair signal intensity ratio analysis (IPSIRA), calculations from the line shift analysis, and the bandwidth analysis. This can prove to be a great tool in future perturbation and near-resonance interaction calculations.

Finally, positions of observed atomic lines were cooperated in the speculation of a couple of discrepencies in the results.

References

[1]W.C. Price, Proc. R. Soc. London, Ser. A **167**, 216 (1938).

[2]R. F. Barrow and J. G. Stamper, Proc. R. Soc. London, Ser. A **263**, 259 (1961).

[3]R. F. Barrow and J. G. Stamper, Proc. R. Soc. London, Ser. A **263**, 277 (1961).

[4]S. G. Tilford, M. L. Ginter, and J.T. Vanderslice, J. Mol. Spectrosc. **33**, 505 (1970).

[5]S. G. Tilford and M. L. Ginter, J. Mol. Spectrosc. **40**, 568 (1971).

[6]D. S. Ginter and M. L. Ginter, J. Mol. Spectrosc. **90**, 177 (1981).

[7]S. G. Tilford, M. L. Ginter, and A. M. Bass, J. Mol. Spectrosc. **34**, 327 (1970).

[8]M. L. Ginter, S. G. Tilford, and A. M. Bass, J. Mol. Spectrosc. **57**, 271 (1975).

[9]D. S. Ginter, M. L. Ginter, and S. G. Tilford, J. Mol. Spectrosc. **90**, 152 (1981).

[10]D. S. Ginter, M. L. Ginter, S. G. Tilford, and A. M. Bass, J. Mol. Spectrosc. **92**, 55 (1982).

[11]D. S. Ginter, M. L. Ginter, and S. G. Tilford, J. Mol. Spectrosc. **92**, 40 (1982).

[12]J.B. Nee, M. Suto, and L. C. Lee, J. Chem. Phys. **85**, 719 (1986).

[13]J. B. Nee, M. Suto, and L. C. Lee, J. Chem. Phys. **85**, 4919 (1986).

[14]T. A. Spiglanin, D. W. Chandler, and D. H. Parker, Chem. Phys. Lett. **137**, 414 (1987).

[15]D. S. Green, G. A. Bickel, and S. C. Wallace, J. Mol. Spectrosc. **150**, 303 (1991).

[16] D. S. Green, G. A. Bickel, and S. C. Wallace, J. Mol. Spectrosc. **150**, 354 (1991).

[17] D. S. Green, G. A. Bickel, and S. C. Wallace, J. Mol. Spectrosc. **150**, 388 (1991).

[18]D. S. Green and S. C. Wallace, J. Chem. Phys. **96**, 5857 (1992).

[19]E. de Beer, B. G. Koenders, M. P. Koopmans, and C. A. de Lange, J. Chem. Soc., Faraday Trans. **86**, 2035 (1990).

[20]Y. Xie, P.T. A. Reilly, S. Chilukuri, and R. J. Gordon, J. Chem. Phys. **95**, 854 (1991).

[21]R. Callaghan and R. J. Gordon, J. Chem. Phys. **93**, 4624 (1990).

[22]Á. Logadóttir, M.S. thesis, Iceland, 1997.

[23]Á. Kvaran, H. Wang, and Á. Logadóttir, *Recent Research Developments in Physical Chemistry* (Transworld Research Network, 1998), Vol. 2, pp. 233-244.

[24]S. A. Wright and J. D. McDonald, J. Chem. Phys. **101**, 238 (1994).

[25]S. T. Pratt and M. L. Ginter, J. Chem. Phys. **102**, 1882 (1995).

[26]E. De Beer, W. J. Buma, and C. A. de Lange, J. Chem. Phys. **99**, 3252 (1993).

[27]Á. Kvaran, Á. Logadóttir, and H. Wang, J. Chem. Phys. **109**, 5856 (1998).

[28]Á. Kvaran, H. Wang, and Á. Logadóttir, J. Chem. Phys. **112,** 10811 (2000).

[29]C. Romanescu and H. P. Loock, Phys. Chem. Chem. Phys. **8**, 2940 (2006).

[30]Á. Kvaran, H. Wang, K. Matthíasson, A. Bodi, and E. Jónsson, J. Chem. Phys. **129**, 164313 (2008).

[31]Á. Kvaran, K. Matthíasson, and H. Wang, J. Chem. Phys. **131**, 044324 (2009).

[32]K. Matthíasson, J. Long, H. Wang, and Á. Kvaran, J. Chem. Phys. **134**, 164302 (2011).

[33]H. Haken and H. C. Wolf. *The physics of atoms and quanta – seventh edition. (Springer-Verlag Berlin Heidelberg, Berlin, 2004).* p 55-57 & 118.

[34] The World Wide Web 9.5.2011. http://webbook.nist.gov/chemistry/form-ser.html.en-us.en (NIST - National Institute of Standards and Technology).

[35]Á. Kvaran and H. Wang, Molec. Phys. **100** (22), 3513 (2002).

[36]K. Matthíasson, H. Wang, and Á. Kvaran, J. Mol. Spec. **255** (1), 1 (2009).

[37]Á. Kvaran, K. Matthíasson, and H. Wang, Physical Chemistry; An Indian Journal. **1** (1), 11 (2006).

[38] The World Wide Web 25.5.2011 http://www.phys.ttu.edu/~gglab/rydberg_state.html (Texas Tech University, Department of Physics).

[39]The World Wide Web 26.5.2011 http://www.raunvis.hi.is/~agust/rempisvaedidir/hbrabstand.htm (Heimasíða Ágústs Kvaran)

5 Appendix

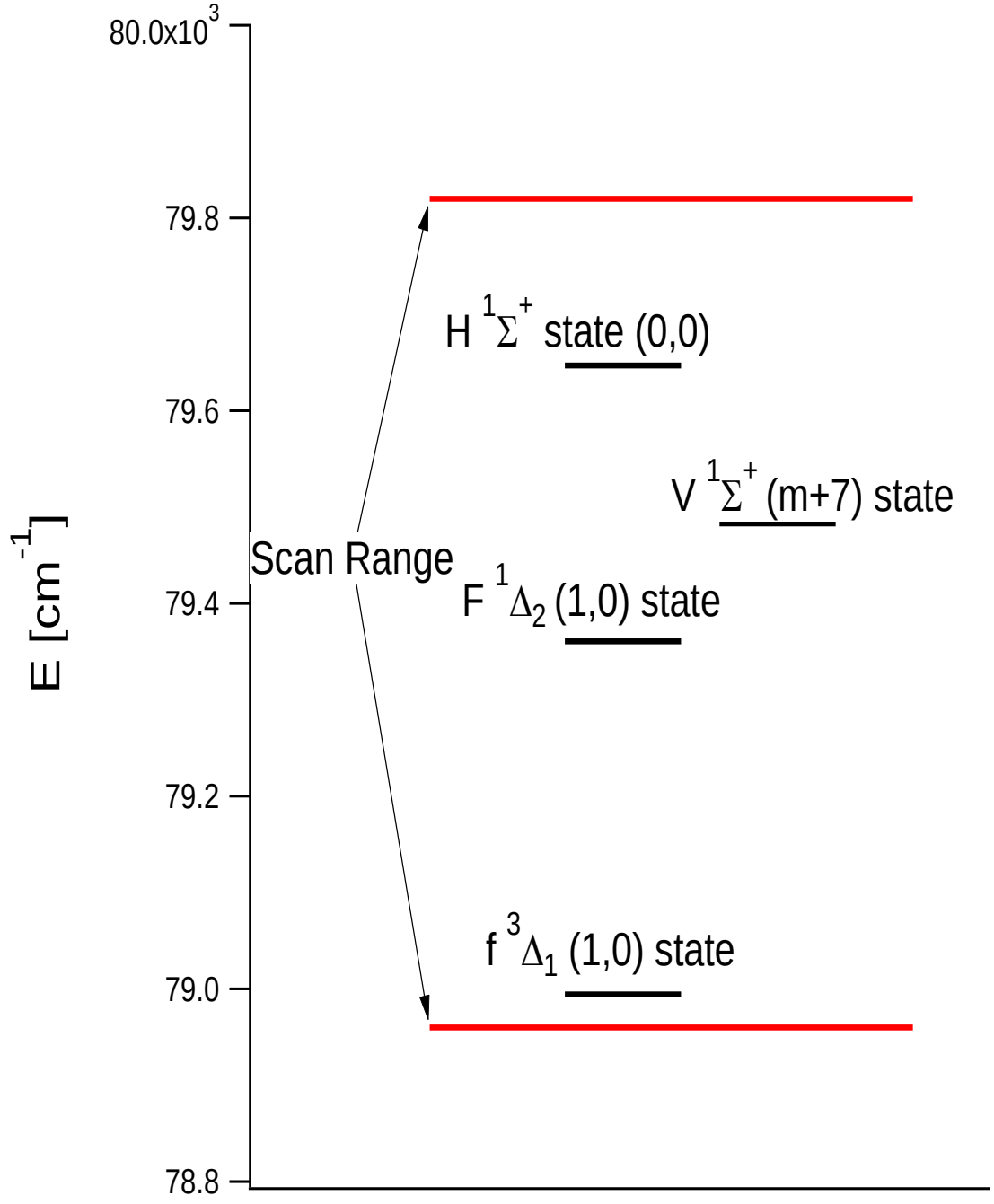

Figure 5-1 Range of the REMPI scan for this particular research and the excited states measured.

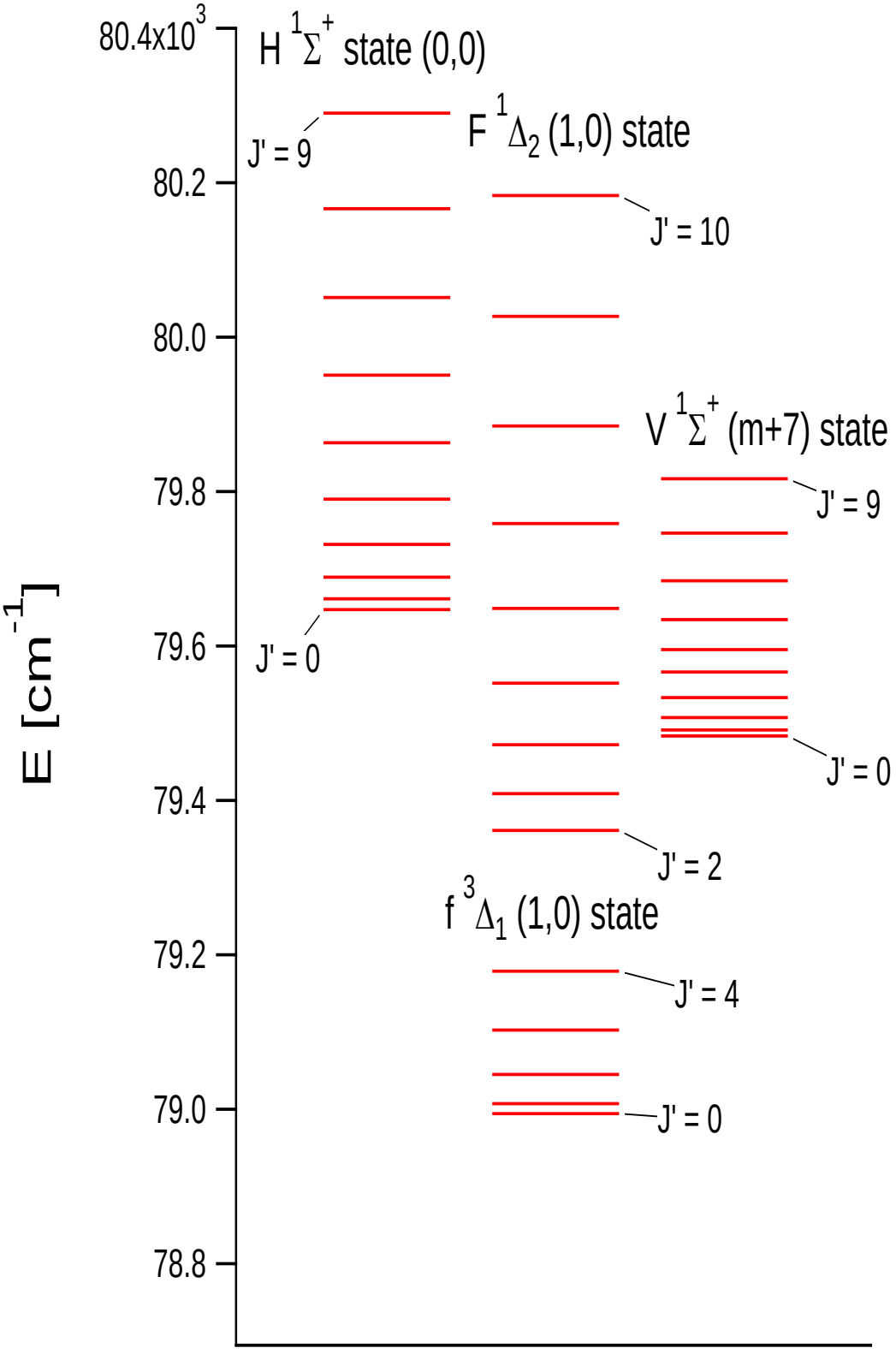

Figure 5-2 Positions of all rotational quantum states observed in this particular research.

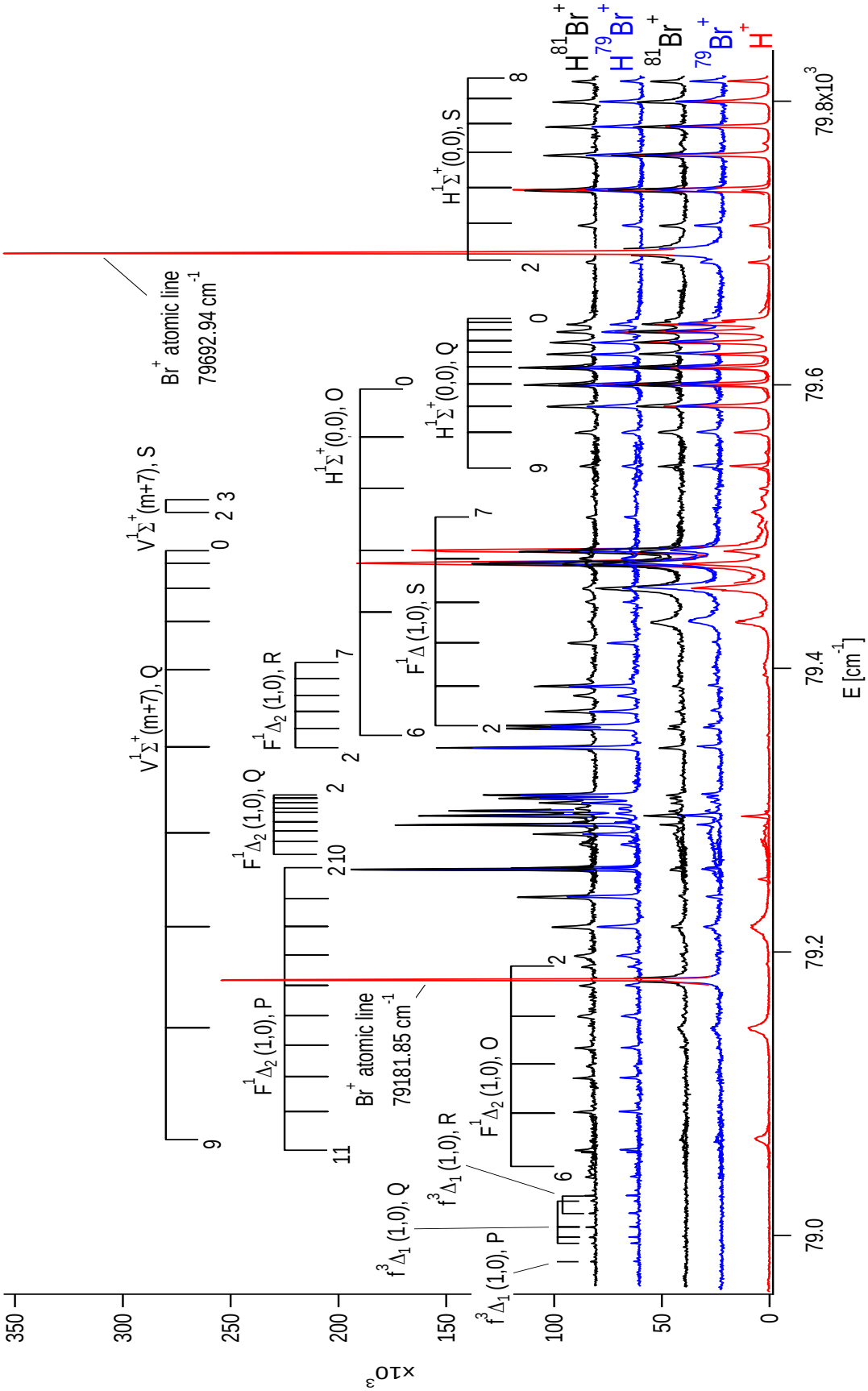

Figure 5-3 1D REMPI overview spectrum of the scanned range for this experiment.

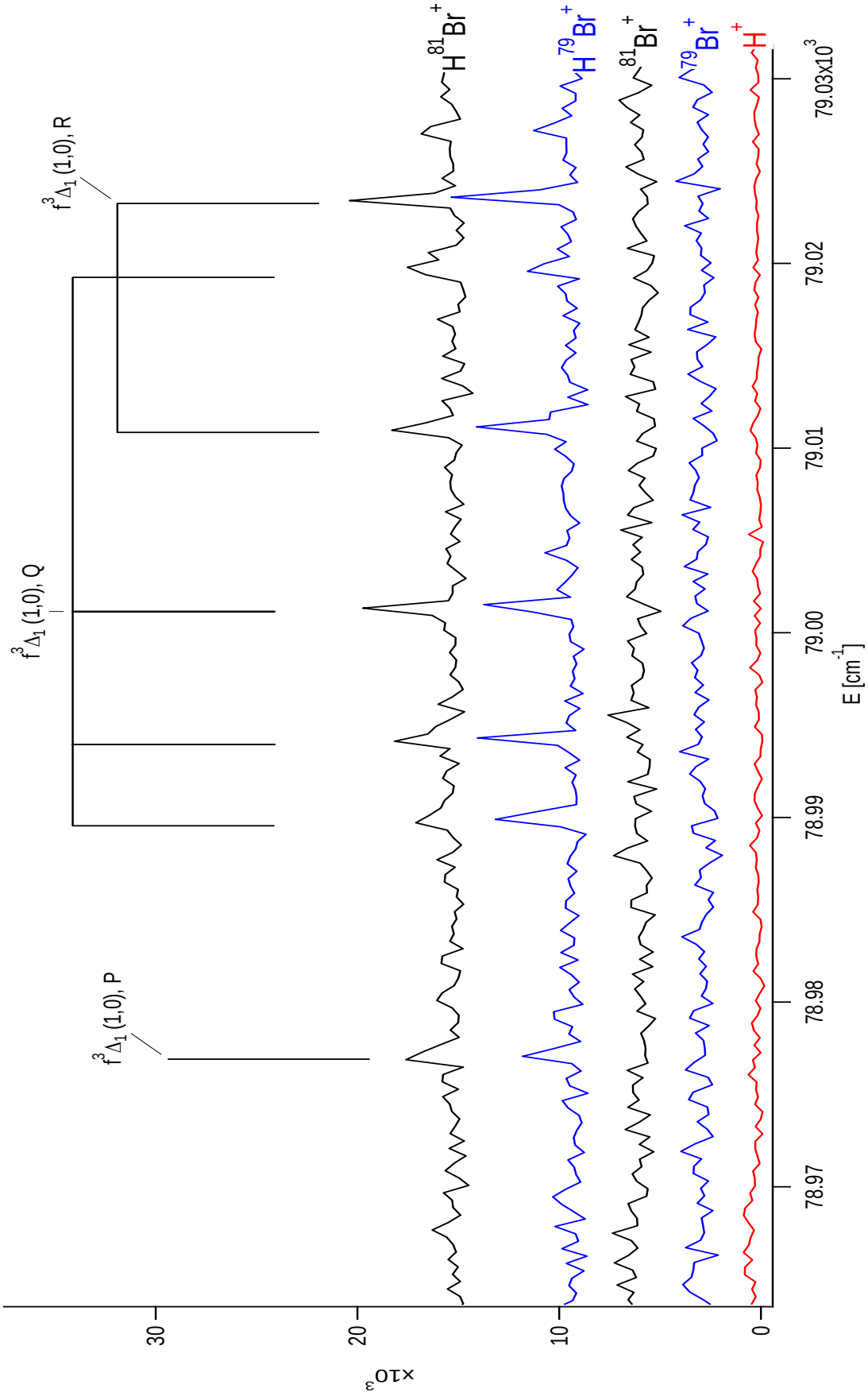

Figure 5-4 Enlarged view of the HBr REMPI spectrum. Pictured is the $f^3\Delta_1$ (1,0) state.

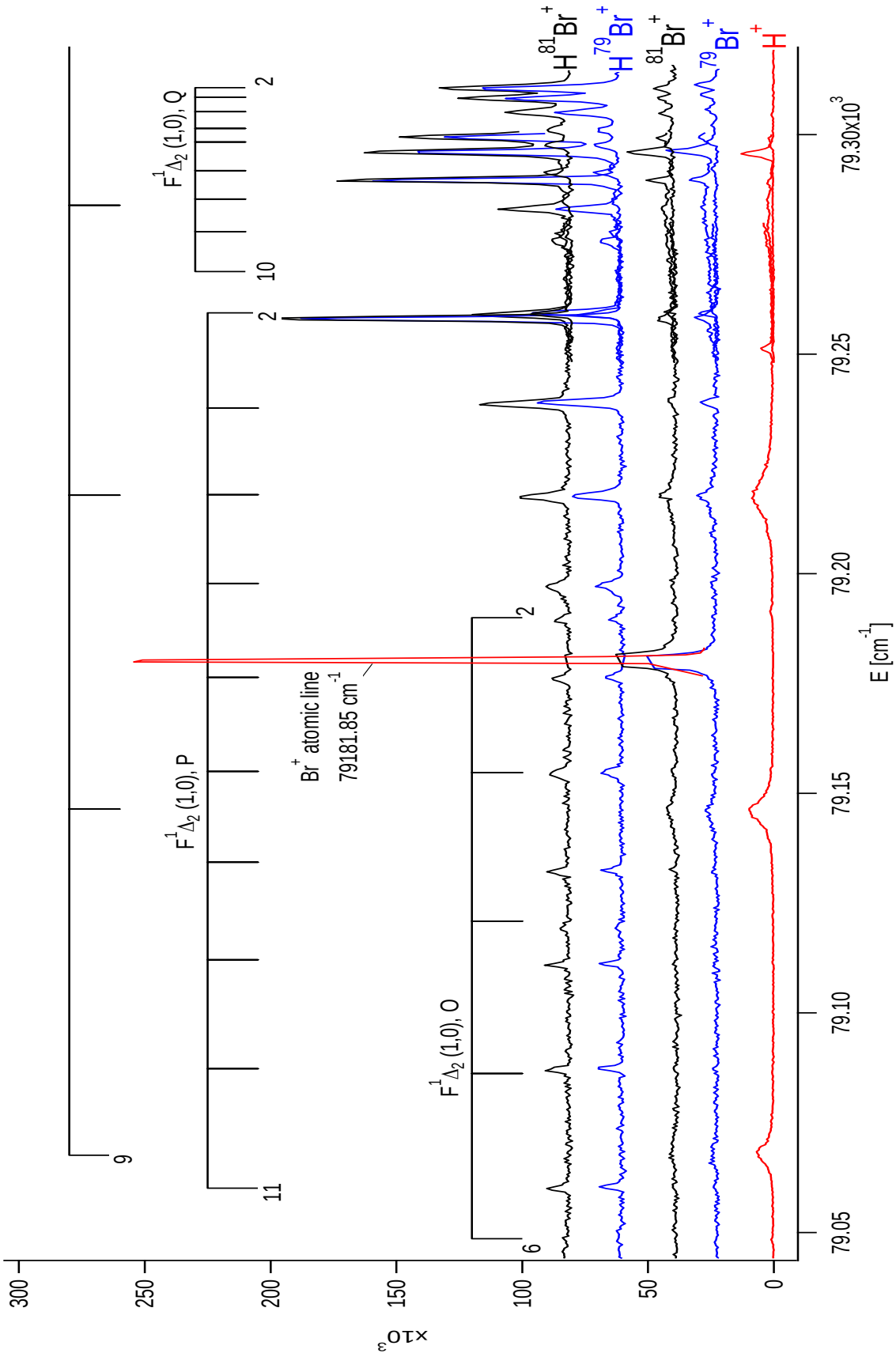

Figure 5-5 Enlarged view of the HBr REMPI spectrum. Pictured are the O, P and Q lines of the $F^1\Delta_2$ (1,0) state and some of the Q lines of the $V^1\Sigma^+$ (m+7) state.

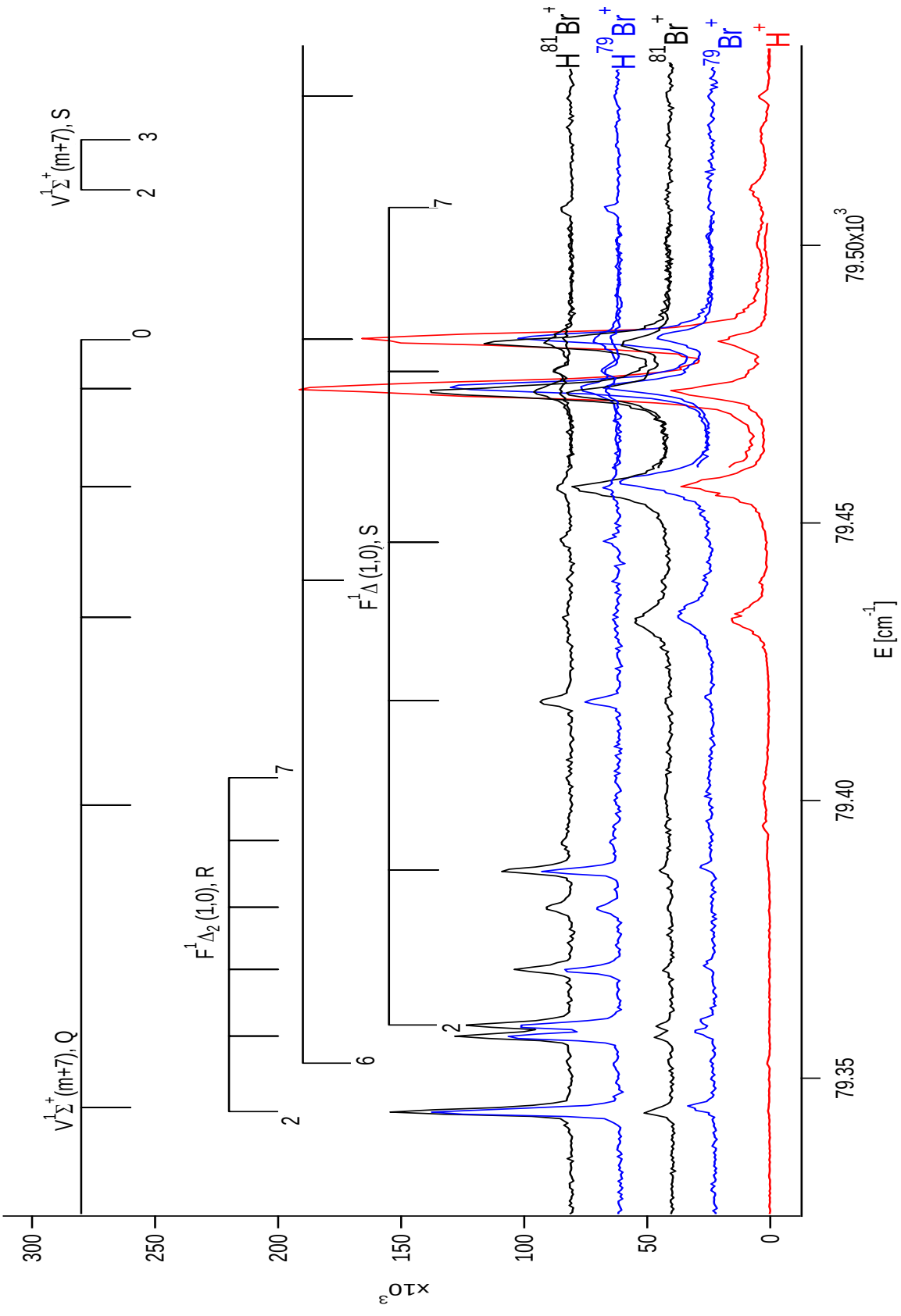

Figure 5-6 Enlarged view of the HBr REMPI spectrum. Pictured are the R and S lines of the $F^1\Delta_2$ (1,0) state, the rest of the Q lines of the $V^1\Sigma^+$ (m+7) state, the S lines of the $V^1\Sigma^+$ (m+7) state and some of the O lines of the $H^1\Sigma^+$ (0,0) state.

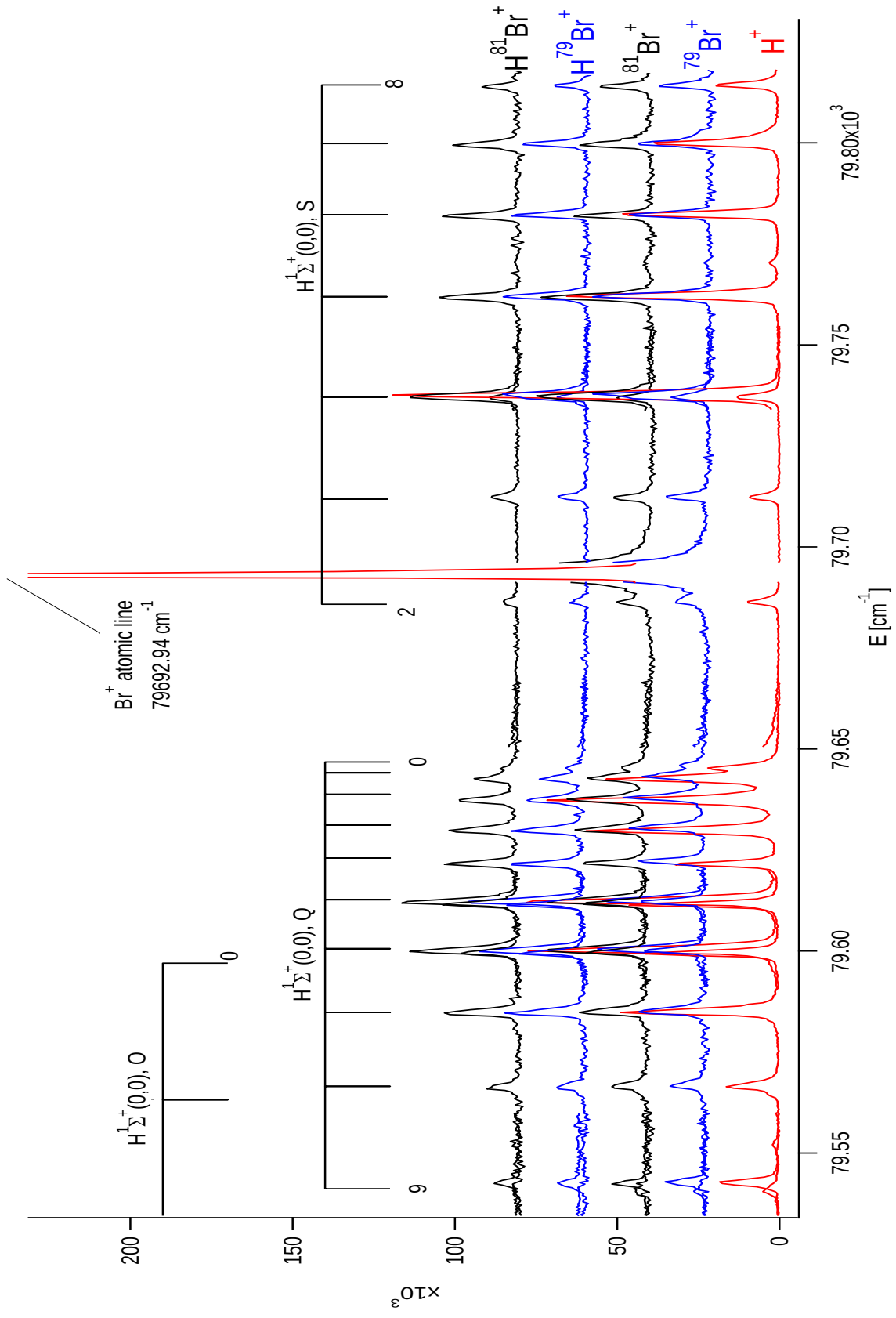

Figure 5-7 Enlarged view of the HBr REMPI spectrum. Pictured are the Q, S and rest of the O lines of the $H^1\Sigma^+$ (0,0) state.